American Mineralogist, Volume 64, pages 1133–1155, 1979

Temperature–composition relationships between naturally occurring augite, pigeonite, and orthopyroxene at one bar pressure

MALCOLM ROSS AND J. STEPHEN HUEBNER

U.S. Geological Survey
Reston, Virginia 22092

Abstract

Natural orthopyroxene crystals containing augite exsolution lamellae were heated at one bar and controlled oxygen fugacity to determine the temperature at which orthopyroxene + augite first react to form pigeonite ± melt. Pigeonite was detected by X-ray precession photography. The reaction to form pigeonite is initiated at the orthopyroxene–augite boundary, probably on the augite lamellae, which are structurally similar to pigeonite and where the orthopyroxene and augite are in chemical equilibrium. The upper temperature limit for the minimum stability temperature of pigeonite at one bar, determined from heating experiments on natural pyroxenes, varies from 1284°C at Mg/(Mg + ΣFe) = 0.92 (atomic), to 901°C and 0.04. Orthopyroxene which does not contain augite exsolution lamellae, and remains unsaturated with respect to augite component, transforms to pigeonite at the higher temperatures of the orthopyroxene–pigeonite stability field. Partial melting accompanies formation of pigeonite for orthopyroxene compositions more magnesian than Mg/(Fe+Mg) = 0.55 (atomic).

Introduction

The pyroxene minerals, because of their presence in a wide variety of igneous and metamorphic rocks, are the subject of intense and continuous study by many petrologists, mineralogists, and crystallographers. An understanding of the stability fields of these minerals in terms of temperature, pressure and chemical composition is crucial to understanding the crystallization history of pyroxene-bearing rocks. Of the seven common pyroxenes, jadeite, acmite, omphacite, aegirine–augite, augite, pigeonite, and orthopyroxene, the last three are by far the most important and are the particular subject of this paper. One or more of these three pyroxenes occurs in many terrestrial and lunar igneous rocks and in metamorphic rocks of the pyroxene–hornfels, amphibole–granulite, and granulite facies.

In this paper we give the results of heating experiments at one bar on naturally-occurring orthopyroxenes which contain augite exsolution lamellae. From these experiments we determined the temperatures at which the transformation

$$\text{opx} \pm \text{augite} \rightarrow \text{opx} \pm \text{augite} + \text{pigeonite} \pm \text{liquid}$$

is first observed. This temperature is equal to, or greater than, the minimum temperature for the coexistence of three pyroxenes at one bar and a particular bulk composition. This work has been previously reported in abstract form (Ross *et al.*, 1972; Ross and Huebner, 1975a, b).

The quadrilateral pyroxenes

Definitions

For the purposes of this paper, we consider the "quadrilateral pyroxenes" to be augite, pigeonite, orthopyroxene, and protopyroxene. The chemical composition of these pyroxenes is given by the formula $M_2T_2O_6$. The M sites may contain Ca,Mg,Fe^{2+}, as well as lesser amounts of Fe^{3+}, Li, Na, Mn^{2+}, Ti^{4+}, Cr^{3+}, and Al^{3+} in natural pyroxenes. The T sites contain Si^{4+} and Al^{3+}.

All augites have space-group symmetry $C2/c$. Most augites are in the composition range defined by the following occupancy limits of the M sites:

(1) $Ca + Mg + Fe^{2+} + Na + Fe^{3+} + Al \geqq 1.00$

(2) $100Ca/(Ca + Mg + Fe^{2+}) \geqq 20$

and

(3) $100(Ca + Mg + Fe^{2+})/(Ca + Mg + Fe^{2+} + Na + Fe^{3+} + Al) \geqq 75$

Pigeonites possess space-group symmetry $C2/c$, or $P2_1/c$ at lower temperatures, and have M-site occupancy limits of:

0003–004X/79/1112–1133$02.00

(1) $Ca + Mg + Fe^{2+} \geqq 1.40$
and
(2) $100\,Ca/(Ca + Mg + Fe^{2+}) < 20$

Orthopyroxenes have space group symmetry *Pbca* and M-site occupancy limits of:

(1) $Ca + Mg + Fe^{2+} \geqq 1.40$
and
(2) $100Ca/(Ca + Mg + Fe^{2+}) < 7$

Protopyroxene has not been found to occur naturally but has been synthesized by many workers, usually has the composition $Mg_2Si_2O_6$, and has been referred to as protoenstatite. Ito (1976) was the first to prepare good single crystals of protopyroxene; the composition he synthesized is $Li_xSc_xMg_{2-2x}Si_2O_6$. The space group of Ito's phase is *Pbcn,* based on a full three-dimensional crystal structure analysis (H. T. Evans, Jr., personal communication, 1977; Smyth and Ito, 1977), which verifies the symmetry proposed by Smith (1959) on protopyroxene of the composition $Mg_2Si_2O_6$.

The compositions of pyroxenes are commonly expressed in terms of mole percent $Ca_2Si_2O_6$ (Wo), $Mg_2Si_2O_6$ (En), and $Fe_2Si_2O_6$ (Fs). The amount of these three components depends on the method of normalization of the chemical formula; different methods can give slightly different values. To avoid inconsistencies caused by the use of different pyroxene norms to calculate "Wo," "En," and "Fs" we have chosen to express "quadrilateral" pyroxene compositions using the relationships

(1) $[Ca] = 100Ca/(Ca + Mg + \Sigma Fe)$
(2) $[Mg] = 100Mg/(Ca + Mg + \Sigma Fe)$
and
(3) $[Fe] = 100\,Fe/(Ca + Mg + \Sigma Fe)$

where $Fe = Fe^{2+} + Fe^{3+}$ and Ca,Mg,Fe^{2+}, and Fe^{3+} are the numbers of cations per formula unit. For "quadrilateral" pyroxenes that do not contain large amounts of Al_2O_3, TiO_2, MnO, Fe_2O_3, and Na_2O the [Ca], [Mg], and [Fe] values are close to the values Wo, En, and Fs, respectively, calculated by the various normalization methods.

Occurrences in igneous and metamorphic rocks

Cooling magmas crystallize quadrilateral pyroxenes in a generally consistent sequence of compositions such that the first pyroxenes to crystallize are magnesium-rich and the last are iron-rich. The studies of Wager and Deer (1939), Brown (1957), and Brown and Vincent (1963) establish quantitatively the pyroxene crystallization trend in rocks of gabbroic composition—specifically those of the Skaergaard Intrusion, East Greenland. The "Skaergaard pyroxene trend," now firmly established in the geological literature, commences with coprecipitation of magnesium-rich augite and orthopyroxene followed by coprecipitation of augite and pigeonite; the pyroxenes increase in iron content as fractional crystallization proceeds (Brown, 1957, Fig. 2). This crystallization trend has also been observed in numerous other volcanic and intrusive rocks, such as Bushveld Complex (Atkins, 1969) and the Hakone tholeiitic andesites (Nakamura and Kushiro, 1970b). Some of the most extensive pyroxene fractionation trends are observed in the lunar basalts (summarized by Papike *et al.,* 1976). Some individual pyroxene phenocrysts in the lunar basalts are chemically and structurally zoned so as to reflect the entire pyroxene crystallization trend, the phenocryst cores being magnesium-rich pigeonite, the rims iron-rich augite (Boyd and Smith, 1971).

The association augite–orthopyroxene is found most typically in granulite-facies metamorphic rocks, but also in some pyroxene–hornfels and transitional amphibolite–granulite rocks. The chemical compositions of the coexisting pyroxenes in granulite-facies rocks having a variety of bulk compositions have been carefully described by a number of geologists, including Binns (1962) on granulites from the Broken Hill district of New South Wales, Subramaniam (1962) on charnockites and associated granulites from various localities, Davidson (1968) on granulites of the Quairading district, Western Australia, Immega and Klein (1976) on iron formation, and Rietmeijer (1979) on iron-rich igneous rocks in Norway. Coexisting orthopyroxene and augite also occur in lunar metamorphic rocks such as the Apollo 15 anorthosite 15415 (Stewart *et al.,* 1972), the Apollo 17 troctolite 76535 (Gooley *et al.,* 1974), and the noritic breccia 77215 (Huebner *et al.,* 1975). Petrographic and chemographic evidence suggests that the orthopyroxene and augite were equilibrated in these rocks.

Equilibrium assemblages containing orthopyroxene and pigeonite are apparently quite rare, for these two phases in the presence of melt coexist only over a very narrow compositional range. Virgo and Ross (1973) reported on coexisting orthopyroxene and pigeonite phenocrysts in Mull andesite glass but could not demonstrate true equilibrium relationships. The three-phase assemblage orthopyroxene–pigeonite–augite is also quite rare: basaltic or andesitic magmas are in equilibrium with three pyroxenes only over very restricted temperature–composition ranges. In strongly fractionating liquids, however, the

melt may intersect the three-pyroxene field over an appreciable temperature–composition range where orthopyroxene, pigeonite, augite, and melt are in reaction relation (Huebner *et al.,* 1972). Examples of three coexisting pyroxenes have been reported in andesites from Weiselberg, Germany and Hakone volcano, Japan by Nakamura and Kushiro (1970a, b).

Protopyroxene has not been reported as occurring naturally; however, evidence exists that a magnesium-rich pigeonite ("clinoenstatite") found in porphyritic volcanic rocks from Cape Vogel, Papua (Dallwitz *et al.,* 1966) and in the Shaw L-group chondrite (Dodd *et al.,* 1975) is an inversion product from high-temperature protopyroxene.

Subsolidus reactions

An example of the subsolidus pyroxene phase relations is depicted in Figure 1, a planar section through the pyroxene ternary phase volume, and coincident with an orthopyroxene–augite tie line. Augite and pigeonite which coprecipitate above the three-pyroxene stability region and then cool slowly will unmix pigeonite and augite, respectively. Pigeonite on cooling into the two-phase augite–orthopyroxene stability volume may transform to the stable assemblage augite plus orthopyroxene, thereby forming so-called "inverted pigeonite" (Huebner *et al.,* 1975). "Inverted pigeonite" generally occurs in the more slowly cooled intrusive rocks such as those of the Skaergaard, Bushveld, Duluth, and Stillwater intrusions. Alternatively, pigeonite may persist metastably and continue to exsolve augite as in the more rapidly cooled lunar basalt 12021 (Ross *et al.,* 1973). The original augite on continued cooling below the three-pyroxene stability volume either may continue to exsolve pigeonite metastably or may nucleate and begin to unmix the stable orthopyroxene phase.

Orthopyroxene and augite can crystallize stably together below the three-phase region. Unless cooling is very rapid or the initial calcium content is very low, the orthopyroxene will exsolve augite. Even the low-calcium metamorphic orthopyroxenes (0.5 to 1.2 weight percent CaO) invariably contain some exsolved augite (Jaffe *et al.,* 1975). Augite that crystallized below the three-phase region may on cooling unmix stable orthopyroxene, metastable pigeonite, or both (Jaffe *et al.,* 1975).

The availability of naturally-occurring unmixed pyroxenes presents an opportunity to study subsolidus phase relationships by subjecting the pyroxene crystals to stepwise heating experiments. Such experiments were carried out on single crystals of

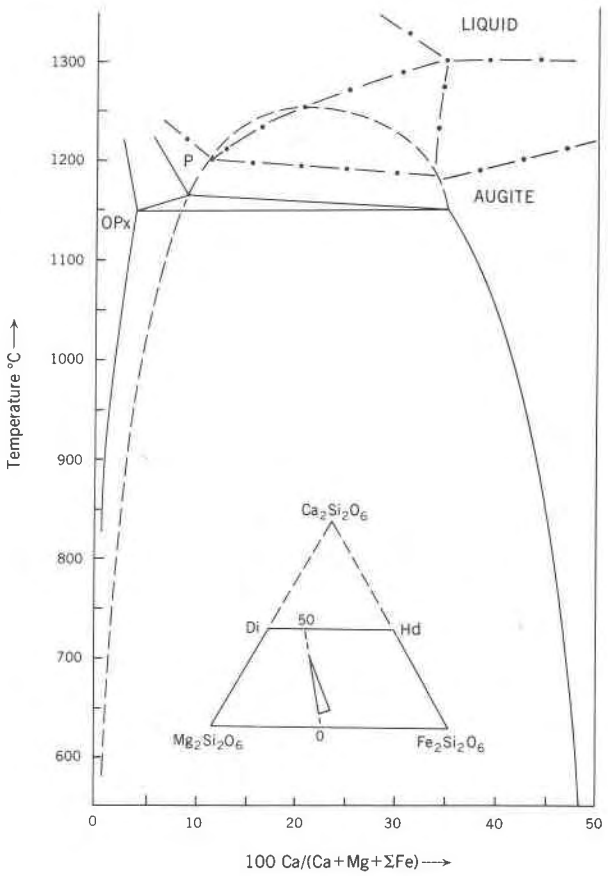

Fig. 1. Temperature–composition section along the pyroxene quadrilateral join $[Ca]_0[Mg]_{66}[Fe]_{34}$–$[Ca]_{50}[Mg]_{38}[Fe]_{12}$ (inset) which is drawn to be coincident with an orthopyroxene–augite tie line at granulite-facies metamorphic temperatures. This join very closely approximates a binary system at temperatures below the three-pyroxene region (~1150°C). Elsewhere the section is pseudobinary. Fields shown are sections through ternary phase volumes. Solid lines—stable subsolidus elements. Dashed line—metastable subsolidus elements. Dot–dash lines—solidus and liquidus relationships. OPx=orthopyroxene, P=pigeonite, Di=$CaMgSi_2O_6$, Hd=$CaFeSi_2O_6$.

augite and pigeonite from a lunar basalt (Ross *et al.,* 1973). In that study, the augite–pigeonite solvus and temperature of first melting were delineated by means of experimental techniques similar to those used in this work.

Orthopyroxene heating experiments

Previous work

Earlier investigations do not establish the conditions at which naturally occurring orthopyroxene + augite react to form pigeonite. Neither of the two previous comprehensive studies took into account the Ca-, Fe-, and Mg-bearing components which must

all be considered together when discussing natural pyroxenes. In the first study, Yang (1973) presented runs in the iron-free system CaO–MgO–Al_2O_3–SiO_2 that bracket what is probably the orthopyroxene–augite–pigeonite equilibrium. These results, which will be discussed later, cannot be directly applied to the Fe-bearing natural pyroxenes. In the second investigation, Bowen and Schairer (1935) presented a phase diagram (their Fig. 8) which depicts the phase relations of synthetic pyroxene on the join $Mg_2Si_2O_6$–$Fe_2Si_2O_6$ at one bar. Included in this diagram is an orthopyroxene–clinopyroxene transition loop which was delineated from heating experiments on six naturally-occurring orthopyroxenes. Their clinopyroxene is pigeonite as we now define it. The other parts of their Figure 8 need not concern us here other than to mention that they report that the pyroxene solidus in the pure system $Mg_2Si_2O_6$–$Fe_2Si_2O_6$ is 200 to 300°C above the OPx–CPx transition loop and that olivine and tridymite may appear as reaction products upon heating of very iron-rich orthopyroxenes.

Two other studies give a clue to the temperatures at which natural (Ca-, Mg-, and Fe-bearing) orthopyroxene might be expected to react to form augite. Smyth (1969) studied a heated single crystal of orthopyroxene of composition [Fe] = 70 by X-ray film methods. At 1050±25°C, the crystal inverted slowly to pigeonite and did not react back to orthopyroxene at lower temperatures. We do not know whether he first heated the orthopyroxene at lower temperatures and found no reaction. Brown (1968) found that at less than 1 bar, a natural pyroxene having an approximate composition $Ca_{0.154}Mg_{0.882}Fe_{1.024}Si_2O_6$, and consisting of orthopyroxene with coarsely exsolved augite ("inverted" pigeonite), did not react to pigeonite during runs of 7 to 17 days unless heated to 1200°C. Upon addition of andesitic melt flux, Brown was able to lower the reaction temperature to 1000°C, and to reverse the reaction at 990°; but changes in the pyroxene composition, which undoubtedly took place by means of cation exchange with the melt, are unknown.

Characterization of samples studied

Thirty natural orthopyroxenes were used in our heating experiments. Their chemical compositions are given in Table 1; all contain negligible amounts of Na_2O, Cr_2O_3, and TiO_2, and only moderate amounts of CaO (0.2 to 2.5 weight percent), MnO (0 to 3.6 weight percent), and Al_2O_3 (0 to 2.0 weight percent) with the exception of sample 30 which contains 8 weight percent Al_2O_3. The $Mg/(Mg + \Sigma Fe)$ ratio in these orthopyroxenes ranges from 0.917 to 0.046, encompassing nearly the entire range found in natural orthopyroxenes.

Orthopyroxene crystals 0.1 to 0.5 mm long and of good optical quality were selected for the heating experiments. All crystals, except those from samples 29 and 30, contain augite exsolution lamellae oriented on the (100) plane of the host (Table 2). The augite lamellae can usually be detected optically, as well as in most single-crystal X-ray precession photographs of the $h0l$ net. Typical orthopyroxene crystals containing lamellar inclusions of augite are shown in Figures 2A and 2B. The amount of augite in the single-crystal mode of the host orthopyroxene crystals (Table 2) is estimated from the intensity of the 402 and $\bar{6}02$ reflections of augite which appear adjacent to the 902 and $\bar{9}02$ reflections, respectively, of orthopyroxene. The detection limit by the X-ray precession method is about 1 mole percent augite oriented within the host phase.

The formation of pigeonite in a heated crystal is signaled by the appearance of the 002 and $00\bar{2}$ pigeonite reflections adjacent to the 202 and $\bar{2}02$ (or $\bar{2}02$ and $20\bar{2}$) orthopyroxene reflections, respectively (Fig. 3A, B). The pigeonite, as will be shown later, commonly grows epitaxially at the interface of the augite lamellae and orthopyroxene host, thereby precluding optical distinction of pigeonite lamellae formed on heating from augite lamellae originally present. At higher temperatures appropriate to the composition, all the orthopyroxene is converted to pigeonite (Fig. 3C). As it is equally probable that pigeonite will orient with respect to the orthopyroxene in either one of the two possible (100) twin configurations, two sets of $h0l$ pigeonite reflections usually appear in the precession photographs.

The accuracy of the estimated single-crystal modes (Ross *et al.*, 1973, p. 623) as obtained from visually-read X-ray intensities is difficult to assess. We estimate that as little as one mole percent pigeonite can be detected in the heated crystals. In a sequence of heating experiments on the same crystal, we can distinguish between 1 and 2 percent pigeonite, 15 and 20 percent pigeonite, or 40 and 50 percent pigeonite in orthopyroxene. We can also compare this method of estimating crystal modes with values determined by measuring the areas of high-calcium (augite) and low-calcium (pigeonite and/or orthopyroxene) pyroxene in photomicrographs of coarsely unmixed augite and pigeonite crystals from the Wyatt Harbour Complex, Labrador. Agreement between the X-ray and optical methods for four unheated crystals

Table 1. Chemical formulas of naturally-occurring orthopyroxenes[1] used in heating experiments[2]

Sample No.	1	2	3	4	5	6	7	8	9	10	11	12	13	14	15	16	17	18	19	20
Si	1.963	1.985	1.974	1.969	1.974	1.981	1.963	1.933	1.986	1.980	1.969	1.958	1.934	1.946	1.961	1.996	1.955	1.986	1.940	1.996
Al	0.058	0.055	0.042	0.066	0.075	0.066	0.083	0.079	0.042	0.068	0.068	0.017	0.057	0.060	0.061	0.003	0.051	0.005	0.001	0.000
Cr^{3+}	0.014	0.013	0.011	-	-	-	-	0.020	-	-	-	0.025	0.005	0.000	0.002	0.000	0.000	0.000	0.000	0.000
Ti	0.000	0.000	0.001	0.003	0.002	0.003	0.004	0.003	0.005	0.004	0.006	0.004	0.003	0.002	0.008	0.000	0.000	0.000	0.000	0.000
Fe^{3+}[2]	0.004	0.000	0.000	0.005	0.000	0.000	0.000	0.035	0.000	0.000	0.000	0.037	0.066	0.044	0.001	0.000	0.039	0.023	0.119	0.008
Fe^{2+}	0.157	0.162	0.235	0.245	0.262	0.272	0.272	0.234	0.348	0.387	0.438	0.456	0.451	0.575	0.839	0.860	0.875	1.083	1.058	1.101
Mn	0.003	0.003	0.006	0.007	0.007	0.000	0.005	0.006	0.007	0.007	0.013	0.017	0.011	0.018	0.019	0.042	0.040	0.037	0.037	0.125
Mg	1.789	1.768	1.718	1.631	1.639	1.644	1.635	1.591	1.575	1.521	1.472	1.451	1.420	1.336	1.060	1.080	1.013	0.839	0.815	0.741
Na	0.000	0.000	0.000	0.013	0.000	0.000	0.000	0.004	0.000	0.000	0.000	0.001	0.002	0.000	0.003	0.000	0.000	0.000	0.000	0.000
Ca	0.011	0.014	0.012	0.060	0.041	0.034	0.038	0.094	0.036	0.033	0.034	0.035	0.051	0.019	0.046	0.021	0.027	0.027	0.030	0.029
Σ charges[2]	12.000	12.038	12.001	12.000	12.027	12.034	12.017	12.000	12.022	12.036	12.018	12.000	12.000	12.000	12.000	12.000	12.000	12.000	12.000	12.000
[CA][3]	0.6	0.7	0.6	3.1	2.1	1.7	1.9	4.8	1.8	1.7	1.7	1.8	2.6	1.0	2.4	1.1	1.4	1.4	1.5	1.5
[MG][3]	91.4	90.9	87.4	84.0	84.4	84.3	84.1	81.4	80.4	78.4	75.7	73.3	71.4	67.7	54.5	55.1	51.8	42.5	40.3	39.4
[FE][3]	8.0	8.3	12.0	12.9	13.5	14.0	14.0	13.8	17.8	19.9	22.5	24.9	26.0	31.4	43.2	43.9	46.8	56.1	58.2	59.0
Mg/Mg+ΣFe	0.917	0.916	0.880	0.867	0.862	0.858	0.857	0.855	0.819	0.797	0.771	0.746	0.733	0.683	0.558	0.557	0.526	0.431	0.409	0.401
Ref.[4]	L	M	J	A	A	A	A	B	A	A	A	C	D	E	B	F	E	F	F	F
Field No.	H-1	SP-1	82436	J-1	J-8	16-276	61-46	61-SC	15-2117	15-1248	US-9	JM-1	N5	A21	53NB	277	J223	264	278	207S
% Quad[5] Components	97.9	97.2	98.3	96.8	97.1	97.5	97.3	96.0	98.0	97.1	97.2	97.1	96.1	96.5	97.3	98.1	95.8	97.5	95.2	93.6

Sample No.	21	22	23	24[1]	25	26	27	28	29	30
Si	1.954	1.961	1.996	2.006	1.958	1.937	1.977	1.957	1.991	1.809
Al	0.033	0.013	0.006	0.019	0.018	0.019	0.013	0.024	0.018	0.331
Cr^{3+}	0.000	0.000	0.000	0.001	0.000	0.002	0.003	0.003	0.000	0.000
Ti	0.002	0.001	0.000	0.004	0.000	0.003	0.004	0.004	0.000	0.000
Fe^{3+}[2]	0.054	0.063	0.000	0.023	0.066	0.097	0.020	0.055	0.000	0.058
Fe^{2+}	1.260	1.440	1.530	1.480	1.664	1.646	1.753	1.761	0.350	0.301
Mn	0.035	0.063	0.030	0.025	0.005	0.044[6]	0.048[7]	0.068[8]	0.007	0.003
Mg	0.632	0.409	0.418	0.360	0.256	0.221	0.150	0.088	1.623	1.488
Na	0.001	0.002	0.000	0.003	0.000	0.000	0.000	0.006	0.000	0.007
Ca	0.030	0.049	0.008	0.079	0.033	0.032	0.033	0.035	0.012	0.003
Σ charges[2]	12.000	12.000	12.000	12.000	12.000	12.000	12.000	12.000	12.000	12.000
[CA][3]	1.5	2.5	0.4	4.1	1.6	1.6	1.6	1.8	0.6	0.2
[MG][3]	32.0	20.9	21.2	18.5	12.7	11.1	7.7	4.5	81.8	80.4
[FE][3]	66.5	76.6	78.4	77.4	85.7	87.3	90.6	93.7	17.6	19.4
Mg/Mg+ΣFe	0.325	0.214	0.213	0.193	0.148	0.113	0.078	0.046	0.823	0.806
Ref.[4]	E	G	H	N	O	E	E	E	I	K
Field No.	Ca-17	2	9B	W2-1678	XYZ	Po-13	SC-6	Po-17	107387	Codera
% Quad[5] component	96.1	94.9	97.8	96.0	97.7	95.0	96.8	94.2	99.3	89.5

[1] Except for sample no. 24 which is a pigeonite which has partly reacted to form augite plus orthopyroxene (partly "inverted" pigeonite).

[2] Formulas are based on Σ cations = 4.000. If the Σ charges <12.000 assuming no ferric iron is present, ferric iron is added to the formula to bring this sum to exactly 12.

[3] [CA] = 100Ca/Ca+Mg+ΣFe, [MG] = 100Mg/Ca+Mg+ΣFe, [FE] = 100ΣFe/Ca+Mg+ΣFe.

[4] References: (A) Bushveld complex (Cameron, 1963), X-ray fluorescence analysis (Desborough and Rose, 1968); (B) Stillwater complex, E.D. Jackson, wet chemical analysis by L. Beatty and L. Schocker (61-SC) and R.E. Stevens (53NB), U.S.G.S.; (C) Johnstown meteorite (Mason and Jarosewich, 1971), wet chemical analysis by Jarosewich; (D-O) electron probe analyses by J.S. Huebner and N. Hickling, U.S.G.S.; (D) Stillwater complex, S.K. Saxena; (E) metamorphics of Massachusetts and New York (Jaffe et al., 1975); (F) metamorphosed iron formation, Quebec (Butler, 1969); (G) granite, Rubideaux Mt., Calif. (Larsen and Draisin, 1950); (H) metamorphosed Wabush Iron formation, Labrador (Klein, 1966); (I) USNM #107387, India; (J) pyroxenite, Webster, N.C., USNM #82436; (K) sapphirine-bearing rock, Val Codera, Italy (Barker, 1964); (L) pyroxenite, Webster, N.C., C.S. Ross; (M) pyroxenite, Spruce Pine, N.C., C.S. Ross; (N) anorthosite, Nain, Labrador (Smith, 1974); (O) charnockite gneiss, Isortog Fiord, W. Greenland (Ramberg and Devore, (1951).

[5] mole percent "quad components" $CaSiO_3$+$MgSiO_3$+$FeSiO_3$

[6,7,8] Includes, respectively, 0.014, 0.018, and 0.020 atoms of Zn.

Table 2. Crystal modes and run conditions for orthopyroxene single-crystal heating experiments

Sample Number	$[Fe]_i$ / $([Fe]_i)$ [4]	Crystal Mode [2]			Run Conditions [3]			
		% Pig	% Aug	Others	T°C	Time(h)	-log atm fO_2	a_{FeO}
1	8.0	0	3	-	25	0		
	(7.7)	0	2	-	1264	41	12.41	0.05
		0	2	-	1272	50	8.61	0
		0	2	-	1284	70	8.55	0
		2	1	-	1284	473Rp	8.42	0
2	8.3	0	3	-	25	0	-	-
	(8.0)	2	2	-	1269	186	10.68	0
3	12.0	0	3	-	25	0	-	-
	(11.5)	0	2	-	1247	18	9.36	0.04
		5	2	-	1259	329	9.1	0.05
		5	2	ℓ?	1271	187	8.80	0.06
		3	2	-	1281	41	12.17	0.06
		10	1	ℓ	1332	71	8.26	0.05
4	12.9	0	3	-	25	0	-	-
	(13.0)	1	3	ℓ?	1243	18	11.77	0.05
		0	2	-	1246	25	11.39	0
		10	1	-	1274	25	11.17	0
		10	1	ℓ	1275	25Rp	11.15	0
		15	0	ℓ	1310	21	10.70	0
5	13.5	0	2	-	25	0		
	(13.0)	0	1	ℓ?	1214	72	11.83	0
		0	2	-	1235	20	11.73	0
		1	2	-	1243	66	11.70	0
		5	2	-	1254	51	11.79	0.11
		10	1	ℓ	1274	25	11.17	0
		15	0	ℓ	1310	21	10.70	0
6	14.0	0	3	-	25	0		
	(13.8)	1	2	-	1246	25	11.39	0
		10	1	ℓ	1274	25	11.17	0
		10	1	-	1189	97Rv	12.12	0
		10	1	-	1179	812Rv	12.31	0
7	14.0	0	2	-	25	0		
	(13.8)	1	1	-	1232	44	12.0	0
		10	1	ℓ	1275	25	11.15	0
		15	1	-	1310	21	10.70	0
8	13.8	0	7	-	25	0		
	(13.8)	0	5	-	1214	72	11.83	0
		1	5	-	1232	44	12.0	0
		3	6	ℓ	1243	96	11.94	0.11
		20	5	ℓ	1274	25	11.17	0
		20	5	-	1246	25Rv	11.39	0
		20	2	-	1281	41	12.17	0.06
9	17.8	0	3	-	25	0		
	(17.5)	0	2	-	1200	126	12.36	0
		1	2	-	1214	72	11.83	0
		5	2	-	1246	25	11.39	0
		5	2	-	1199	43Rv	11.39	0
		5	0	-	1189	97Rv	12.12	0
		5	0	-	1179	812Rv	12.31	0
		15	1	ℓ	1274	25	11.17	0
		15	1	ℓ ?	1275	25Rp	11.15	0
		15	1	ℓ	1310	21	10.70	0
10	19.9	0	4	-	25	0		
	(19.5)	0	3	-	1199	43	11.93	0
		2	3	ℓ?	1211	67	11.98	0
		15	3	-	1214	72	11.83	0
		15	1	-	1188	115Rv	12.19	0
		15	1	-	1179	812Rv	12.31	0
		20	0	-	1275	25	11.15	0
		20	0	-	1246	25Rv	11.39	0
11	22.5	0	3	-	25	0		
	(21.8)	10	1	-	1211	67	11.98	0
		2	0	-	1150	87Rv,L	12.81	0
		15	1	-	1214	72	11.83	0
		0	0	-	1188	115Rv,L	12.19	0
12	24.9	0	1	-	25	0		
	(24.3)	0	1	-	1191	21	12.28	0
		2	1	-	1199	43	11.93	0
		3	1	-	1214	18	11.94	0
		5	1	-	1224	181	12.12	0
13	26.0	0	4	-	25	0		
	(25.6)	10	0	ℓ?	1175	74	12.75	0
		5	2	-	1182	50	12.24	0
		20	0	ℓ	1199	43	11.93	0
		0	0	ℓ	1179	812Rv,L	12.31	0
14	31.4	0	2	-	25	0		
	(30.2)	5	2	-	1160	49	12.10	0
		3	0	-	1162	66	12.64	0
		5	2	ℓ	1172	69	12.26	0
		7	2	ℓ	1177	75	12.54	0
15	43.2	0	tr.	-	25	0		
	(42.4)	30	0	-	1150	87	11.15	0
		30	0	-	1130	144Rv	12.86	0
16	43.9	0	tr.	-	25	0		
	(42.4)	0	0	-	1076			
		0	0	-	1110	71	13.26	0
		2	0	-	1118	163	13.48	0
		5	0	-	1130	144	12.86	0
17	46.8	0	1	-	25	0		
	(45.5)	0	0	-	1087	19	12.45	0
		4	1	-	1102	21	13.49	0
		4	1	-	1102	22Rp	13.53	0
		10	0	ℓ?	1130	144	12.86	0
		30	0	ℓ?	1150	87	12.81	0
		30	0	ℓ?	1130	144Rv	12.86	0
		70	0	ℓ	1189	51	12.75	0.44
		70	0	-	1050	289Rv		
		100	0	-	1221	25	12.21	0.52
		100	0	ℓ	1226	54	11.59	0.26

Table 2. (continued)

Sample Number	[Fe]1/ ([Fe]$_i$)4/	Crystal Mode % Pig	% Aug	Others	Run Conditions3/ T°C	Time(h)	-log atm fO_2	a_{FeO}
18	56.1	0	tr.	-	25	0		
	(55.0)	0	0	-	1022	93	11.94	0
		1	0	-	1038	168	14.36	0
		5	0	-	1050	139	14.39	0
		8	0	-	1076	44	13.87	0
		90	0	-	1110	71	13.26	0
		100	0	-	1130	144	12.86	0
19	58.2	0	tr.	-	25	0		
	(57.0)	1	0	-	1022	93	14.94	0
		15	0	Fa	1042	43	14.80	0.46
		85	0	-	1050	139	14.39	0
		90	0	-	1076	44	13.87	0
20	59.0	0	tr.	-	25	0		
	(58.0)	0	0	-	1020	21	14.95	0
		15	0	-	1036	20	14.69	0
		95	0	ℓ	1050	139	14.39	0
		98	0	ℓ	1076	44	13.87	0
21	66.5	0	1	-	25	0		
	(65.2)	0	0	-	997	24	15.14	0
		1	0	-	1003	64	15.32	0
		100	0	-	1020	164	14.8	0
22	76.6	0	tr.	-	25	0		
	(76.0)	0	1	-	890	120	17.53	0
		0	0	-	952	137	16.12	0
		2	0	-	972	67	15.67	0
		5	0	-	985	44	15.32	0
		8	0	-	1000	89	15.12	0
		98	0	Crist(1) Fa(1)	1050	289	14.38	0
23	78.4	0	tr.	-	25	0		
	(76.0)	0	0	-	933	122	16.38	0
		0	0	-	952	137	16.12	0
		1	0	-	960	94	16.01	0
		98	0	Crist(1) Fa(1)	985	44	15.32	0
24	77.4	50	35[5]	-	25	0		
	(77.4)	50	35	-	952	42	14.6	0
		65	35	-	965	141	15.04	0.40
		62	30	-	965	141	15.04	0.40
		30	50	Crist(10) Fa(10)	1050	125	13.79	0.33
25	85.7	0	1	-	25	0		
	(84.0)	0	0	-	933	122	16.38	0
		2	0	Crist(1) Fa(1)	960	94		
		10	0	Crist(10) Fa(10)	985	44	15.32	0
26	87.3	0	3	-	25	0		
	(86.0)	1	2	-	901	290	16.14	0.44
		2	1	Crist(1) Fa(1)	965	140	15.29	0.30
27	90.6	0	tr.	-	25	0		
	(89.5)	(100% Crist + Fa)			965	141	15.04	0.40
28	93.7	0	4	-	25	0		
	(92.8)	1	2	-	901	290	16.14	0.44
		(100% Crist. + Fa)			965	93	15.05	0.38
29	17.6	0	0	-	25	0		
	(16.5)	0	0	-	1367	25	8.60	0.02
		100	0	-	1382	67L	8.04	0.04
30	19.4	0	0	-	25	0		
	(18.3)	0	0	-	1310	21	10.70	0
		75	0	ℓ	1364	23L	10.20	0

1/ [Fe] = 100ΣFe/(Ca+Mg+ΣFe)

2/ Estimated mole percent of all crystalline phases from X-ray precession photographs. Aug - augite, Pig - pigeonite, Fa - fayalite, Crist - cristobalite, ℓ - liquid, tr. - trace

3/ Rp - repeated run, Rv - reversal run, L - iron loss from crystal noted

4/ [Fe]$_i$ is the value of 100Fe/(Ca+Mg+Fe) for orthopyroxene thought to be in equilibrium with both pigeonite and augite.

5/ Partly "inverted" pigeonite host which contains 15 mole% orthopyroxene at room temperature. The orthopyroxene begins to react to pigeonite between 952 and 965°C (952 <T_iC <965).

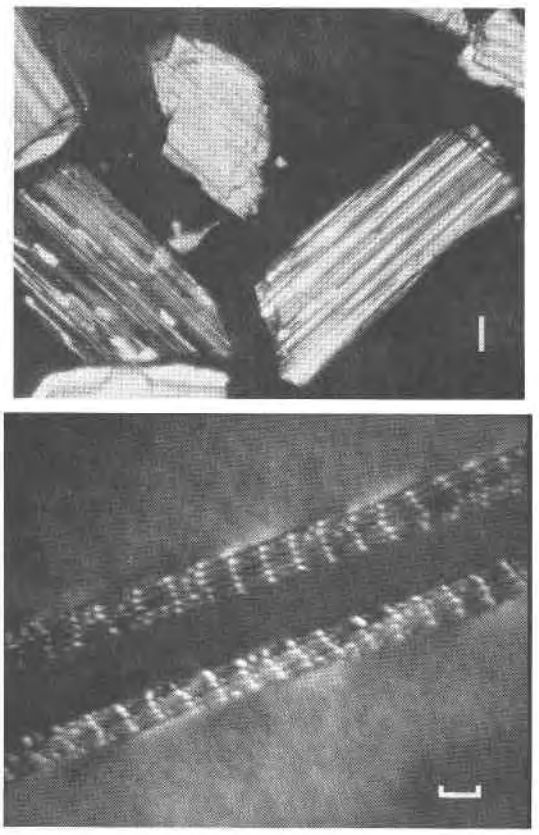

Fig. 2. Orthopyroxene containing exsolution lamellae of augite oriented on (100) of the host. (A) Optical photomicrograph of individual orthopyroxene crystals, crossed polarizers, oil mount, sample 8 (Tables 1, 2). White bar is 0.1 mm. (B) Dark-field transmission electron micrograph (200 kV) of ion-thinned orthopyroxene. Note the large number of periodic interface dislocations along the boundaries (marked by arrows) between augite (dark center band) and orthopyroxene (upper and lower gray areas). Sample 3; crystal was quenched from 947°C. Scale is 0.1μ.

varying in augite content from 30 to 70 mole percent was within 5 mole percent.

In a few X-ray photographs of heated orthopyroxene crystals, diffuse streaks were observed in the positions where the 002 and $00\bar{2}$ pigeonite reflections should be (Fig. 3D). We interpret these diffuse reflections as being due to the formation of pigeonite lamellae 1 to 5 unit-cells thick in the a^* direction.[1] When the crystals showing such streaking were reheated to a slightly higher temperature the streaks were replaced by sharp pigeonite diffraction maxima, indicating that the lamellae had thickened considerably.

Phases other than pyroxene that may also form at the higher heating temperatures include olivine, cristobalite, protopyroxene, and melt. The crystalline phases can be easily detected in the precession photographs. The melt phase, when present in amounts greater than about 1 volume percent, can be detected by carefully examining thinned and polished crystals by means of conventional light optical microscopic techniques. The modes of the heated orthopyroxene crystals and the run conditions are given in Table 2.

Heat treatment

Each orthopyroxene crystal was wrapped loosely in platinum, platinum–iron alloy, or iron foil, heated to the desired temperature in a gas-flow furnace at a controlled (and measured) value of the oxygen fugacity appropriate to maintain the bulk composition of the sample, and quenched to about 5°C in chilled mercury, nominally in one second. The crystals were then photographed by the X-ray precession method.

Platinum-wound quenching furnaces and CO_2 + H_2 gas trains were used as described previously (Ross *et al.*, 1973) but, because iron diffuses rapidly from sample to platinum foil when melt is present, additional steps were taken to prevent loss of iron through the melt to the foil (Huebner, 1973; Huebner *et al.*, 1976). Iron–platinum alloy foil containers were used in many of these runs to specify the iron activity of the system. Judiciously chosen alloy compositions and furnace oxygen fugacity (f_{O_2}) values specified wüstite activity values that are nearly equal to that inherent in the silicate samples, preventing appreciable gain or loss of iron. Uncertainties in furnace gas f_{O_2} determinations (see Huebner, 1975) and in the thermodynamics of the iron–platinum alloys (Heald, 1967), and the lack of thermochemical data for pyroxene solid solutions prohibited calculation of the necessary wüstite activity values; such values were originally determined by trial and error for representative pyroxene bulk compositions. One notable feature of this technique, not possible for runs in evacuated silica-glass tubes, is that f_{O_2} can be treated as an independent variable, in general chosen to maintain the ratios Fe^{2+}/Fe^{3+}, Cr^{2+}/Cr^{3+}, or Ti^{3+}/Ti^{4+} close to their original values.

Orthopyroxenes were heated for at least 18 hours before quenching. By repeating runs on the same crystal for various lengths of time, we ascertained that 18-hour heating periods were usually sufficient to establish whether phase changes would occur at

[1] Discrete diffraction maxima rather than semicontinuous diffuse streaks begin to appear when the lamellar precipitates are greater than 5 unit cells thick (Ross, 1968, Fig. 4).

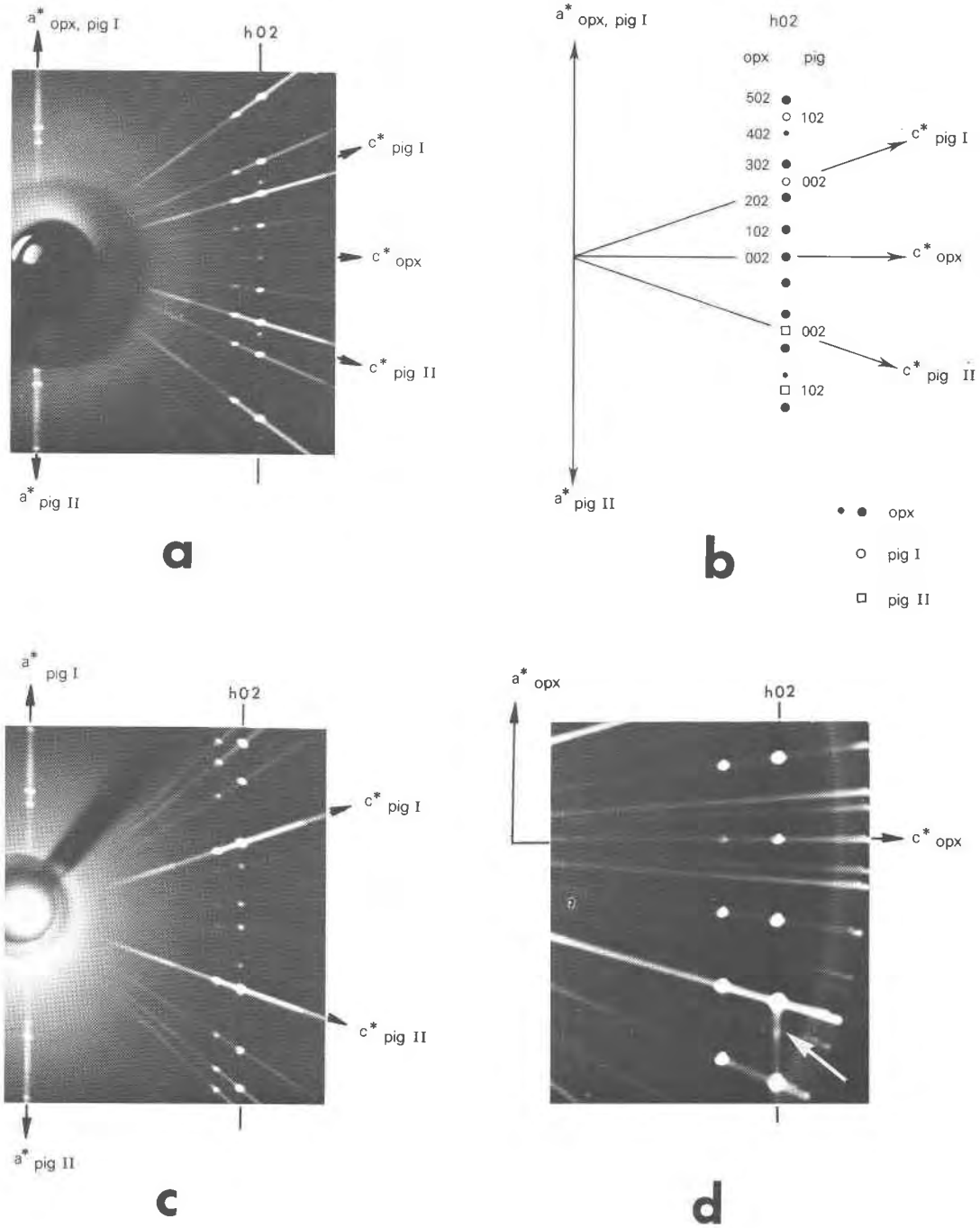

Fig. 3. (A) *h0l* X-ray precession photograph (unfiltered Mo X-radiation) of an orthopyroxene crystal (sample 17, Tables 1, 2) held at 1102°C for 43 hours. The crystal has reacted to form about 4 mole percent pigeonite twinned on (100). The two twin orientations are designated pigeonite I (P I) and pigeonite II (P II). OPx=orthopyroxene. (B) Reproduction of (A) showing the indexing of the reflections. (C) *h0l* X-ray precession photograph (unfiltered Mo X-radiation) of an orthopyroxene crystal (sample 17, Tables 1, 2) held at 1226°C for 54 hours. The orthopyroxene has reacted completely to form pigeonite twinned on (100) plus a small amount of liquid (glass). (D) *h0l* precession photograph (unfiltered Cu X-radiation) of an orthopyroxene crystal (sample 18, Tables 1, 2) held at 1038°C for 168 hours. Diffuse streaking about the 002 reflection position of pigeonite is shown by an arrow.

the interface between the orthopyroxene host and the augite lamellae at a given temperature.

The microprobe analysis procedure used is that described by Huebner *et al.* (1976), "Method One." It must be emphasized that the microprobe analyses of unheated pyroxenes in Table 1 are, to the extent practical, analyses of the orthopyroxene exclusive of the augite lamellae. The wet-chemical analyses generally give greater values for calcium content because the wet-chemical method gives the bulk compositions of the orthopyroxene crystals including all intergrown augite.

Retention of composition

The representative analyzed runs listed in Table 3 and plotted in Figure 4 are evidence that when melt was absent pyroxene single crystals neither lost iron to pure platinum foil, nor gained iron from iron foil, during this study. Especially convincing are the long runs maintained at low oxygen fugacity values for the subsolidus investigation discussed later. The sets of runs in platinum and in iron foil each scatter uniformly about the line of constant composition in Figure 4, indicating that bulk composition was retained. One might have expected the runs in platinum to have shown systematic loss of iron, and the runs in iron to have gained iron as FeO, but they did not. The observed scatter is random and is instead an indication of the analytical level of significance; analysis of the data yields a standard deviation of the measured composition equal to Mg/(Mg + ΣFe) = 0.015.

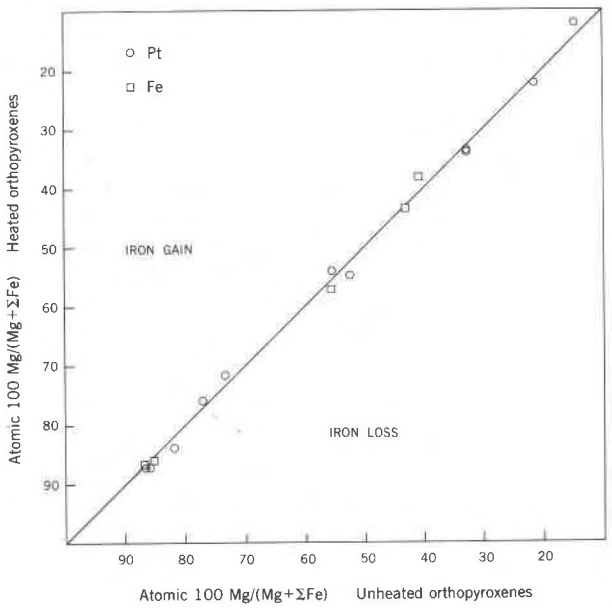

Fig. 4. Mg/(Mg+ΣFe) of heated pyroxene crystals in Table 3 plotted against their respective bulk compositions listed in Table 1. Circles indicate runs made in platinum foil; squares designate runs in iron foil. Points cluster closely about the theoretical line of constant composition. Neither set of runs is biased toward either iron loss or iron gain, suggesting that the observed scatter is related to the precision of the microprobe chemical analyses, not to a change in bulk composition.

Table 3. Subsolidus runs demonstrating retention of bulk composition

Sample No.	Initial OPx Mg/(Mg+ΣFe)	T, °C	Time (h)	Container	Δlog f_{O_2} [1]	Product OPx Mg/(Mg+ΣFe)
4	0.867	1246	24.5	Pt	-0.04	0.872
4	0.867	1168	122.5	Fe	-0.64	0.868
6	0.858	1179	812	Pt	-0.14	0.872
8	0.855	1168	122.5	Fe	-0.64	0.866
8	0.855	1168.5	117	Fe	-1.37	0.861
9	0.819	1179	812	Pt	-0.14	0.840
11 [2]	0.771	1310	21	Pt	-0.08	0.761
13	0.733	1182	50	Pt	-0.11	0.717
16	0.557	1042	43	Fe	-0.68	0.572
16	0.557	1188	115	Pt	-0.13	0.540
17	0.526	1130	144	Pt	-0.03	0.547
18	0.431	1042	43	Fe	-0.01	0.435
19	0.409	1042	43	Fe	-0.68	0.382
21	0.325	1020	163.5	Pt	-0.3	0.337
21	0.325	1057	89.5	Pt	-0.33	0.335
21	0.325	1057	89.5	Pt	-0.33	0.340
22	0.214	1000	89	Pt	-0.31	0.223
25	0.148	935	121.5	Pt	-0.42	0.121

[1] Δlog f_{O_2} = [log f_{O_2} (run)] -[log f_{O_2} iron-wüstite buffer]

[2] Analysis of clear core of single crystal. Margin lost iron (Mg/(Mg+ΣFe)=0.933) and reacted to form protopyroxene.

For bulk compositions more magnesian than Mg/(Mg + ΣFe) = 0.55, the reaction of orthopyroxene + augite to form pigeonite sometimes was accompanied by partial melting. Because sample mass was small relative to that of the metal container, the problem of iron loss (or gain) was potentially severe. The experiments reported in Table 4 and plotted in Figure 5 demonstrate that the use of platinum–iron alloy foil and controlled f_{O_2} can effectively maintain the bulk composition of pyroxenes that have undergone a small amount of partial melting. Within analytical uncertainty [estimated to be ±0.01 in Mg/(Mg + ΣFe) in solids, ±0.015 in melt], the tie line or tie triangle connecting the projected compositions of the run products passes through or encloses the initial pyroxene bulk composition used in each experiment, indicating that the bulk composition was retained.

Obviously, it was not practical to analyze by electron microprobe each crystal after each heating run.

Table 4. Representative experiments demonstrating retention of bulk composition in presence of partial melt

Sample No.	T, °C	Time(h)	log f_{O_2}	a_{FeO}	Phase[1]	Mode[2]	[Ca]	[Mg]	[Fe]
8	1300	44	-11.75	0.08	Pxn	95	1.9	86.1	12.0
					Melt	5	31.8	49.0	19.2
3	1332	71	-8.26	0.05	Opx	85	0.6	87.9	11.5
					Pig	10	5.7	86.1	8.2
					Melt	5	38.9	47.8	13.3
7	1226	53.5	-11.59	0.26	Pig	90	1.0	52.1	46.8
					Olivine	3	0.3	44.2	55.5
					Melt	7	9.2	17.4	73.4
17	1178	52	-12.06	0.30	Pxn	95	1.3	52.6	46.1
					Melt	5	14.0	16.8	69.1

[1] Pxn - orthopyroxene or orthopyroxene-pigeonite mixture

[2] Volume percent, estimated optically and by microprobe traverse

Besides being tedious and consuming much time, the preparation of a polished flat surface requires removal of pyroxene, which changes the shape of the crystal. In our opinion, changing the shape of the crystal would introduce an unacceptably high level of uncertainty into our technique of comparing the X-ray intensity "modes" of a crystal subjected to successive heat treatments.

As a check for iron loss or gain, we determined from the X-ray precession photographs the lattice parameters of the host crystal after each heat treatment. Comparison of the unit-cell dimensions of heated with unheated orthopyroxene crystals (Table 5) suggests that there are no major changes in bulk chemical compositions during successive heating experiments. If the Mg/(Mg + ΣFe) composition ratio of

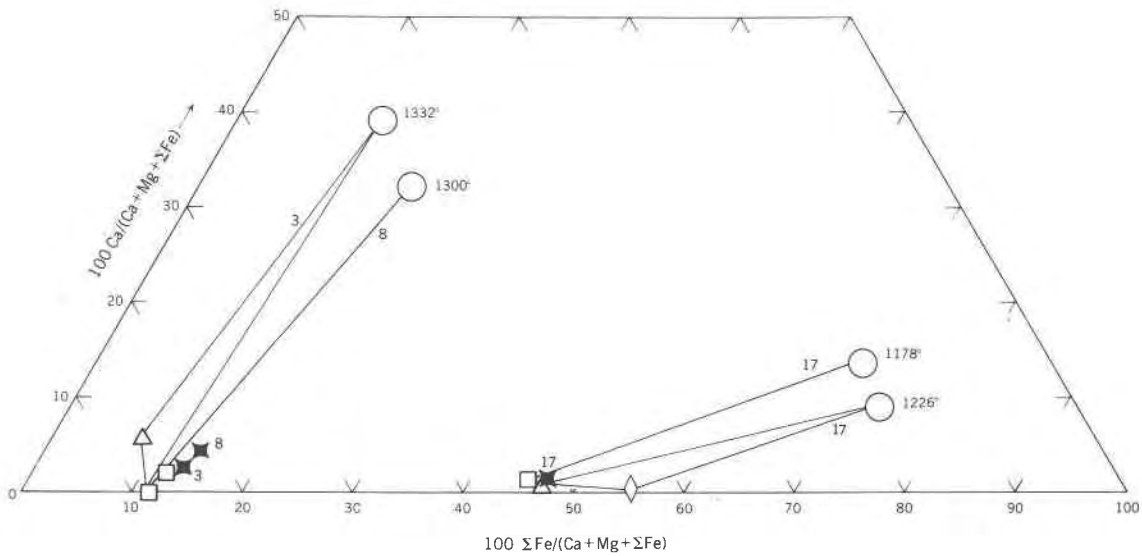

Fig. 5. Composition data for selected orthopyroxene crystals that were partially melted in platinum–iron alloy foil at controlled oxygen fugacity, demonstrating retention of bulk composition (see Table 4). Squares: orthopyroxene or orthopyroxene–pigeonite mixture; triangles: pigeonite; diamonds: olivine; circles: melt compositions; solid symbols: initial orthopyroxene bulk compositions (from Table 1). Compositions of individual phases are projected onto the pyroxene quadrilateral plane on the basis of the total Ca, Mg, and Fe present. Calcium-poor pyroxene forms >90 percent (by volume) of each crystal. Initial bulk compositions (same sample numbers as in Table 1) plot close to the respective bulk compositions of the run products. If iron was lost or gained, the effect is so small that it is obscured by chemical analytical uncertainty.

Table 5. Unit-cell parameters for host orthopyroxene (Opx) before heating (25°C) and for orthopyroxene and pigeonite (Pig) in crystals quenched from temperatures near T_i (Table 2)

Sample Number	Phase	a(Å)	b(Å)	c(Å)	β°	T°C
1	Opx	18.20	8.805	5.174	90	25
	Opx	18.20	8.823	5.190	90	1284Rp
	Pig	9.646	8.823	5.177	108.6	1284Rp
2	Opx	18.24	8.807	5.190	90	25
	Opx	18.24	8.804	5.179	90	1269
	Pig			5.179	108.2	1269
3	Opx	18.25	8.827	5.191	90	25
	Opx	18.25	8.843	5.195	90	1259
	Pig	9.667		5.202	108.5	1259
	Opx	18.24	8.81	5.203	90	1332
	Pig	9.64	8.81	5.227	108.9	1332
4	Opx	18.24	8.844	5.188	90	25
	Opx	18.26	8.840	5.197	90	1243
	Pig		8.840		108.3	1243
	Opx	18.26	8.835	5.199	90	1275
	Pig	9.675	8.835	5.202	108.3	1275
5	Opx	18.24	8.835	5.193	90	25
	Opx	18.27	8.830	5.208	90	1243
	Opx	18.26	8.848	5.196	90	1274
	Pig	9.697	8.848	5.199	108.3	1274
6	Opx	18.26	8.827	5.191	90	25
	Opx	18.24		5.193	90	1246
	Pig				108.1	1246
	Opx	18.27	8.857	5.202	90	1274
	Pig	9.673	8.857	5.200	108.3	1274
7	Opx	18.24	8.850	5.195	90	25
	Opx	18.26	8.830	5.197	90	1232
	Pig		8.830		108.4	1232
	Opx	18.25	8.830	5.197	90	1275
	Pig	9.673	8.830	5.197	108.4	1275
8	Opx	18.24	8.850	5.200	90	25
	Opx	18.24		5.200	90	1243
	Pig			5.208	108.6	1243
	Opx	18.25	8.830	5.200	90	1274
	Pig	9.683	8.830	5.209	108.3	1274
9	Opx	18.26	8.829	5.200	90	25
	Opx	18.24		5.200	90	1214
	Pig				108.3	1214
	Opx	18.24		5.198	90	1246
	Pig	9.660		5.214	108.3	1246
	Opx	18.27	8.833	5.202	90	1274
	Pig	9.663	8.833	5.195	108.4	1274
10	Opx	18.26	8.856	5.205	90	25
	Opx	18.26	8.861	5.207	90	1214
	Pig	9.690	8.861	5.207	108.4	1214
11	Opx	18.27	8.853	5.204	90	25
	Opx	18.28	8.850	5.200	90	1211
	Pig	9.675	8.850	5.208	108.4	1211
	Opx	18.26	8.831	5.199	90	1150Rv
	Opx	18.29	8.865	5.202	90	1214
	Pig	9.963	8.865	5.208	108.4	1214
	Opx	18.23	8.825	5.190	90	1188Rv
12	Opx	18.28	8.866	5.218	90	25
	Opx	18.27	8.865	5.208	90	1214
	Pig				108.5	1214
13	Opx	18.27	8.863	5.209	90	25
	Opx	18.27	8.856	5.204	90	1175
	Pig	9.681	8.856	5.210	108.3	1175
	Opx	18.32	8.865	5.215	90	1199
	Pig	9.716	8.865	5.213	108.3	1199
14	Opx	18.27	8.863	5.207	90	25
	Opx	18.27	8.851	5.206	90	1160
	Pig			5.218	108.6	1160
	Opx	18.30	8.880	5.211	90	1172
	Pig			5.227	108.6	1172
15	Opx	18.28	8.899	5.217	90	25
	Opx	18.33		5.223	90	1130
	Pig			5.235	108.8	1130
	Opx	18.30		5.213	90	1150
	Pig			5.219	108.6	1150
16	Opx	18.30	8.915	5.221	90	25
	Opx	18.28	8.915	5.212	90	1118
	Pig		8.915	5.211	108.7	1118
17	Opx	18.31	8.911	5.217	90	25
	Opx	18.31	8.926	5.224	90	1102
	Pig		8.926	5.227	108.6	1102
	Opx	18.31	8.913	5.199	90	1189
	Pig	9.661	8.913	5.213	108.6	1189
18	Opx	18.35	8.945	5.226	90	25
	Opx	18.31	8.928	5.208	90	1038
	Pig			5.30	108.6	1038
	Opx	18.31		5.213	90	1076
	Pig	9.632		5.234	108.8	1076
19	Opx	18.33	8.967	5.229	90	25
	Opx	18.35	8.958	5.223	90	1022
	Pig			5.243	108.1	1022
20	Opx	18.37	8.977	5.235	90	25
	Opx	18.38	8.990	5.235	90	1036
	Pig	9.713	8.990	5.225	108.6	1036
21	Opx	18.34	8.974	5.232	90	25
	Opx	18.33	8.971	5.231	90	1003
	Pig	9.680	8.989	5.234	108.6	1020
22	Opx	18.40	9.030	5.244	90	25
	Opx	18.41	9.009	5.244	90	972
	Opx	18.40	9.016	5.240	90	1000
	Pig		9.016	5.240	108.9	1000
23	Opx	18.39	9.020	5.228	90	25
	Opx	18.39	9.003	5.223	90	960
	Pig	9.698	9.027	5.222	108.6	985

Table 5. (continued)

Sample Number	Phase	a(Å)	b(Å)	c(Å)	β°	T°C	Sample Number	Phase	a(Å)	b(Å)	c(Å)	β°	T°C
24	Opx	18.38	9.000	5.240	90	25	26	Opx	18.39	9.029	5.242	90	25
	Pig	9.695	9.000	5.240	108.6	25							
	Aug	9.784	9.000	5.253	105.6	25		Opx	18.37		5.239	90	965
								Pig	9.709		5.241	108.4	965
	Opx	18.41	9.013	5.248	90	952							
	Pig	9.707	9.013	5.237	108.6	952	27	Opx	18.44	9.054	5.241	90	25
	Aug	9.791	9.013	5.250	105.7	952							
							28	Opx	18.44	9.056	5.246	90	25
	Pig	9.693	9.000	5.232	108.8	965							
	Aug	9.775	9.000	5.248	105.7	965		Opx	18.43	9.050	5.250	90	901
								Pig			5.254	108.4	901
25	Opx	18.41	9.028	5.244	90	25							
							29	Opx	18.251	8.845	5.198	90	25
	Opx	18.41		5.244	90	960							
	Pig				108.5	960		Opx	18.257	8.868	5.192	90	1367
								Pig	9.598	8.820	5.174	108.4	1382
	Opx	18.44	9.037	5.240	90	985							
	Pig	9.712	9.037	5.248	108.6	985	30	Opx	18.23	8.865	5.189	90	25
								Opx	18.21	8.837	5.198	90	1310
								Pig	9.636	8.822	5.191	108.5	1364

the orthopyroxenes changed during successive runs, this change would be indicated by corresponding changes in the unit-cell edges. The *a* and *b* dimensions of heated crystals listed in Table 5 are, with few exceptions, within 0.02A of the corresponding dimensions of the unheated crystals. From the data of Kuno (1954) for natural orthopyroxenes and Turnock *et al.* (1973) for synthetic orthopyroxenes, a decrease of 0.02A in *a* or *b* would correspond to a 10 percent increase in Mg/(Mg + ΣFe). However, in our experiments, *a* and *b* commonly varied inversely, and in some determinations orthopyroxene in pure platinum foil even yielded dimensions suggestive of the gain of a small amount of iron. We interpret most of the reported changes in *a* and *b* with temperature of heating to be merely random experimental variations attributable to the preparation and measurement of the X-ray precession photographs. Unit-cell dimensions determined by this method have an uncertainty of ±0.2 percent, which accounts for the observed variations. In only five runs (Table 5) did we detect significant evidence for iron loss from the crystal.

Results

The experimental heating conditions and data pertinent to phase characterization of the orthopyroxene crystals are summarized in Tables 2 and 5. The runs for each sample are listed in order of increasing temperature, except for "repeat" and "attempted reversal" runs which are listed immediately after the "initial" run. The same crystal was used for the "initial" and the "repeat" or "attempted reversal" runs. In only one experiment (sample 1, Table 2) did a run repeated at the same temperature show a change in the phase composition (mode) of the crystal. We attempted to reverse the reaction by heating selected crystals at lower temperatures than the previous heating step, but in only two experiments (samples 11, 13) did the amount of pigeonite or augite decrease significantly from that observed in the same crystal at a higher temperature. We cannot be certain that each of these crystals did not lose small amounts of iron during heating, but available unit-cell measurements suggest that such loss is not great (see Table 5). In 13 other attempts no change was observed in the crystal mode.

Pyroxene phase relations

Reaction mechanisms

The three principal subsolidus chemical reactions observed in the orthopyroxene heating experiments are:

(I) homogeneous orthopyroxenes

$$\text{OPx} \rightarrow \text{OPx} + \text{pigeonite}$$

(II) orthopyroxenes containing augite lamellae

$$\text{OPx} + \text{augite} \rightarrow \text{OPx} + \text{pigeonite} + \text{augite}$$

and

(III) orthopyroxenes with [Fe]>75 and containing augite lamellae

$$\text{OPx} + \text{augite} \rightarrow 3 \text{ pyroxenes} \pm \text{fayalite} \pm \text{SiO}_2$$

Two of the three subsolidus pyroxene reaction

paths are shown on Figure 6. First, consider a homogeneous orthopyroxene of composition A. On heating (path I) no change will take place until temperature T_j, where pigeonite of composition F (out of the plane of Fig. 6) starts to crystallize. Heating to even higher temperatures causes more orthopyroxene to react to pigeonite until the three-phase region orthopyroxene + pigeonite + melt is reached.

Next, consider heating an orthopyroxene which contains a few augite lamellae. At the (100) interface the initial compositions of the host and exsolved phases are assumed to be A and B, respectively. If local equilibrium prevails at the interface, the orthopyroxene and augite will readjust compositions along the orthopyroxene and augite solvi (path II). The slower the rate of heating, the greater should be the volume about the interface in which equilibrium prevails. If the augite lamellae are completely dissolved into the host orthopyroxene before temperature T_i is reached, the reaction path changes from type II to type I, and pigeonite eventually forms from a homogeneous orthopyroxene. If augite persists, pigeonite with a composition projected onto the plane of Figure 6 (see inset) will first appear at temperature T_i, at the two-phase interface between orthopyroxene and augite. (As will be discussed later, we have under ideal conditions observed the localization of pigeonite along relict augite lamellae.) As heating continues above T_i, augite will react at the interface, and *locally* the sample will pass into either of the two-phase regions OPx + pigeonite, or pigeonite + augite, depending upon the local activity of the $CaSiO_3$ component. Augite in the central part of the lamellae, not adjacent to the orthopyroxene interface, may not equilibrate during the short heating-run periods that we used. However, persistence of some augite to higher temperatures need not prevent the appearance of pigeonite at T_i.

If equilibrium were to prevail *throughout* those crystals of orthopyroxene which are intergrown with augite lamellae, the following reaction sequences would take place during stepwise heating: (1) in those crystals possessing a bulk composition A (Fig. 6), augite would immediately dissolve and then at T_j orthopyroxene would begin to react to form pigeonite (path I); (2) in crystals having bulk compositions lying between A and C the reaction would follow path II until augite disappeared and then would follow a type I path; (3) in crystals having bulk compositions lying between C and D (for example, some "inverted" pigeonites) the reaction would follow path II, pass through the three-pyroxene region into the orthopyroxene–pigeonite stability volume, and then into the pigeonite stability region; and (4) in crystals slightly more calcic than D ("inverted" pigeonites) the reaction sequence would be the same as (3) except above the three-pyroxene region the reaction path would pass into the pigeonite–augite stability volume and then into the pigeonite stability region, unless melting intervened.

In our experiments, only local equilibrium is likely to prevail. Thus, at the lamellar interface, where the orthopyroxene was saturated with augite, reaction path II prevailed, whereas some distance from the interface, where the host orthopyroxene composition remains unchanged, the reaction mechanism followed path I.

A third type of reaction was observed in the iron-rich orthopyroxenes (samples 22 to 28). At [Fe] = 75–90, we first observed fayalitic olivine and cristobalite in the runs in which we first noted pigeonite, or in the next heating step. Two very iron-rich orthopyroxenes (samples 27 and 28) with [Fe] > 90 ultimately reacted completely to fayalite and cristobalite.

Partial melting

Partial melting of pyroxene was observed in some of the heating experiments for orthopyroxene with $Mg/(Mg+\Sigma Fe) \sim 0.55$ (see also Huebner *et al.*, 1972, 1976). Phase-equilibrium relations involving the partial melting of natural pyroxene bulk compositions are complicated by minor components which depress the solidus by partitioning into a partial melt, enriching it in Al_2O_3 and TiO_2. The $CaSiO_3$ component is also strongly fractionated into the melt. The residue of, for instance, 30 percent partial melting is a very calcium-poor, refractory pyroxene. Because the calcium content of the pyroxene changes on partial melting, we have not reported or discussed experiments in which the amount of melt, estimated by optical methods, exceeded 10 percent by volume of the crystal. Only a small amount of melt, probably less than 2 percent, appeared in some of the crystals at temperatures near T_i. We believe that this melting did not greatly affect our determination of the temperature–composition relations for the three-pyroxene stability region.

Temperatures of reaction to form pigeonite

The run temperatures at which pigeonite was first recognized in the X-ray photographs (Table 2) are given in Table 6 as T_{obs}. In two cases (samples 13 and 20), these temperatures were lowered somewhat because a significant amount of pigeonite (10–35

percent) was estimated to be present at the temperature (T_{obs}) at which it was first observed. The basis for the slight lowering of temperatures is that, other variables being equal, an increasing proportion of pigeonite is correlated with increasing temperature. These two adjusted values of T_{obs} are listed in Table 6. A similar adjustment could have been made for the other samples but was neglected because the correction was only 2–5°C. Also included in Table 6 are the [Ca] and [Fe] values (Table 1) of the unheated orthopyroxenes as well as the expected $[Ca]_i$ and $[Fe]_i$ values for augite-saturated orthopyroxene at T_i (composition C, Fig. 6). The $[Ca]_i$ values are estimated from the composition data given in the literature for orthopyroxenes believed to have crystallized in equilibrium with augite at pressures less than 8 kbar and temperatures at or close to temperatures of maximum calcium saturation (T_i). The $[Fe]_i$ values are obtained from [Fe] values by extrapolating along the appropriate orthopyroxene–augite tie line (see Ross and Huebner, 1975b) from [Ca] to $[Ca]_i$, making the assumption that these tie lines do not rotate appreciably as temperature changes. For the purposes of this paper—where we are more interested in the length of a tie line than in its orientation—this is a reasonable assumption.[2]

The values of T_{obs} for 28 heated orthopyroxene samples are plotted against $[Fe]_i$ in Figure 7. The data for 15 magnesian pyroxenes, which coexisted with augite when pigeonite was first noted, show relatively small scatter. Such a small uncertainty in composition suggests retention of crystal bulk composition during each experiment; had FeO been lost or gained, the observed scatter would undoubtedly have been greater, considering the use of different containers, temperatures, f_{O_2} values, and run durations, each of which would affect differently the rate of iron loss or gain.

Augite was not observed in those runs in which pigeonite was first detected in samples #29 and 30 (Table 2). These samples plot at 1382° and 1360°C, respectively, temperatures that lie considerably above the magnesian orthopyroxene + augite = pigeonite reaction curve (Fig. 7). Because we expect the minimum temperature of pigeonite stability to occur when pigeonite is in equilibrium with *both* orthopyroxene and augite, it is not surprising that these two samples plot well above the reaction curve.

We have not proven that the reaction curve drawn as a solid line in Figure 7, separating fields labelled O+A and O+P±L(±A), is an equilibrium curve because we have not reversed the reaction. Indeed, the detectability limit of the X-ray method precludes observation of pigeonite unless the sample is heated at least several degrees (we estimate 2–5) above the reaction equilibrium. Several lines of reasoning, however, suggest that our curve might not lie far above the equilibrium value: (1) the scatter of points about the reaction curve is small; (2) melt, which would promote the achievement of equilibrium, was observed to be present in some of the plotted runs, and suspected in many runs using samples #1–15; (3) within the limits of uncertainty, our results agree with the reversed determination of the iron-free equilibrium by Yang (1973), discussed in the next section.

Most iron-rich pyroxenes, unlike the magnesian pyroxenes, lost all the augite that was initially present at lower temperatures than those at which pigeonite was observed. In only three cases (samples #17, 26, and 28) was augite present when pigeonite was first observed, thus fulfilling one of the requirements of the equilibrium orthopyroxene + augite $\rightleftarrows$ pigeonite, that all phases be present. In eight cases (samples #16, 18–23, 25) the observed reaction is orthopyroxene $\rightarrow$ pigeonite, which must lie at higher temperatures than the orthopyroxene + augite + pigeonite equilibrium. Most iron-rich pyroxene runs plotted in Figure 7 represent temperatures above the 3-pyroxene equilibrium. Thus the 3-pyroxene curve separating the fields of orthopyroxene + augite and pigeonite is shown as a schematic, dashed line *below* the runs that lost augite. Note that the three runs in which augite was retained (Nos. 17, 26, 28) are, relative to their $[Fe]_i$ value,

[2]Were the exsolved augite to change from Mg/(Fe+Mg) = 100 to 0, the maximum change that is theoretically possible, the coexisting orthopyroxene would change a maximum of 0.06 in Fe/(Fe+Mg). Natural assemblages suggest that the actual degree of rotation is considerably less. We have plotted the orthopyroxene–augite tie lines for about 300 naturally-occurring pairs and find that the slope varies with pyroxene major-element bulk composition but not with rock type (high-temperature basalts, kimberlites, gabbros; intermediate-temperature andesites, iron-rich gabbros, meteoritic rocks; low-temperature granulites, charnockites, granulite–amphibolite transition facies rocks, rhyolites, lunar metamorphic rocks). The observed statistical scatter in tie-line orientation for each rock type obscures any systematic tie-line rotation with changing rock type (changing temperature). We do find that tie-line length increases systematically with decreasing temperature. Thus, we believe that to the first approximation necessary for our purposes, tie-line slopes are nearly independent of the temperature of pyroxene crystallization (Ross and Huebner, 1975b).

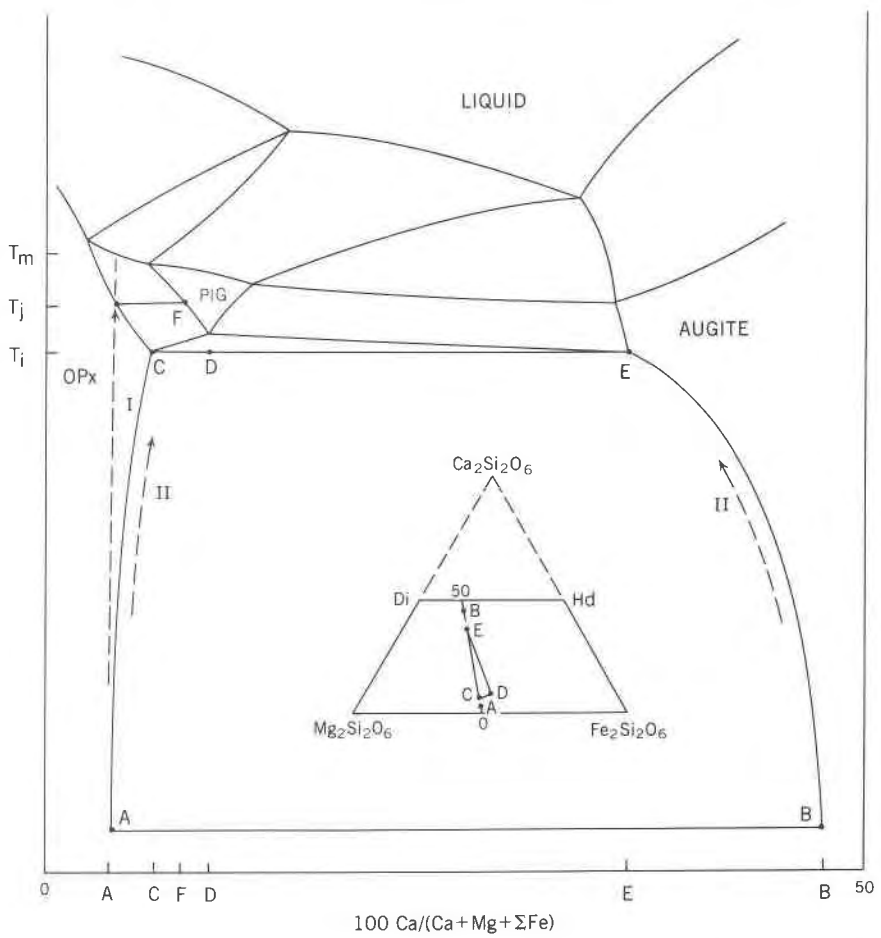

Fig. 6. Planar section through the pyroxene ternary phase volume, T–($Ca_2Si_2O_6$–$Mg_2Si_2O_6$–$Fe_2Si_2O_6$), and coincident with the orthopyroxene–augite tie line AB (inset). The OPx–augite tie lines do not rotate appreciably with temperature, thus the *T–X* section below the three-pyroxene field closely represents the equilibrium compositions. Liquid compositions are taken from Huebner *et al.* (1976). The field boundaries above the temperature of the three-pyroxene field are projected onto the *T–X* section and thus do not depict the actual equilibrium compositions. OPx=orthopyroxenes; P=pigeonite. A, B, C, D, E, F=compositions of phases; T_i=temperature of first appearance of three-pyroxene assemblage (heating path II); T_j=temperature at first appearance of pigeonite in homogeneous orthopyroxene of composition A (heating path I); T_m=temperature of first melting of the orthopyroxene–pigeonite assemblage. Di and Hd have the same meaning as in Fig. 1.

lower in temperature than the other eight runs, with iron-rich samples.

Detailed discussion of two samples

Two series of heating experiments (Samples 3 and 29) will be discussed in detail, because these runs illustrate the interface reaction mechanism and the relationship between temperature and the calcium content of orthopyroxene participating in the reaction OPx → pigeonite. The interface reaction mechanism is illustrated nicely by sample 3, an orthopyroxene of approximate composition $Ca_{0.012}Mg_{1.748}Fe_{0.252}Si_2O_6$ which contains lamellae of augite 7 to 20 micrometers thick. Microprobe analysis suggests that calcic amphibole may be present in a few grains of the pyroxene separate, but amphibole could not be detected by X-ray precession methods. Compositions of the run products for representative samples, summarized in Table 4 and plotted in Figure 5, show that the bulk composition did not change (see also Huebner *et al.*, 1976, Table 2a for complete chemical analyses). Pigeonite was observed in run products heated to 1259°C and above. Melt was observed at 1305° and 1332°C, and may well have first formed at lower temperatures, yet not have been detected optically. The run at 1332°C demonstrates that augite lamellae reacted with adjacent orthopyroxene to form pigeonite + melt

Table 6. Temperature–composition relationships for orthopyroxenes

Sample No.	[Ca][1]	[Fe][1]	[Ca]$_i$[2]	[Fe]$_i$[3]	T°C[4] obs pig
1	0.6	8.0	4.4	7.7	1284
2	0.7	8.3	4.4	8.0	1269
3	0.6	12.0	4.3	11.5	1259
4	3.1	12.9	4.3	13.0	1243
5	2.1	13.5	4.3	13.0	1243
6	1.7	14.0	4.3	13.8	1246
7	1.9	14.0	4.3	13.8	1232
8	4.8	13.8	4.3	13.8	1232
9	1.8	17.8	4.2	17.5	1214
10	1.7	19.9	4.2	19.5	1211
11	1.7	22.5	4.2	21.8	1211
12	1.8	24.9	4.1	24.3	1199
13	2.6	26.0	4.1	25.6	1165
14	1.0	31.4	4.0	30.2	1160
15	2.4	43.2	3.8	42.4	1150
16	1.1	43.9	3.8	42.4	1118
17	1.4	46.8	3.8	45.5	1102
18	1.4	56.1	3.6	55.0	1038
19	1.5	58.2	3.6	57.0	1022
20	1.5	59.0	3.6	58.0	1025
21	1.5	66.5	3.5	65.2	1003
22	2.5	76.6	3.3	76.0	972
23	0.4	78.4	3.3	76.0	960
25	1.6	85.7	3.2	84.0	960
26	1.6	87.3	3.2	86.0	901
27	1.6	90.6	3.1	89.5	none
28	1.8	93.7	3.0	92.8	901
29	0.6	17.6	4.2	16.5	1382
30	0.2	19.4	4.2	18.3	1364

[1] Low temperature compositions (Table 1)

[2] Assumed [Ca] value for calcium-saturated orthopyroxene at temperature T_i° and 1 atmosphere pressure

[3] Slight adjustment of [Fe] values given in third column for expected values at T_{obs}.

[4] Temperature at which pigeonite first observed in the x-ray photographs (Table 2). See text for comment on runs 13 and 20).

(Fig. 5). Optical, X-ray, and microprobe chemical analyses, all performed on the same crystal, revealed that pigeonite and glass (quenched melt) occur exclusively in thin lamellae, lenses, or blebs oriented along or close to the (100) orthopyroxene–augite interfaces (Fig. 8).

Most orthopyroxenes with optically visible augite exsolution lamellae contain interface dislocations formed to relieve the strain between the host and precipitate built up during cooling. These dislocations, examples of which are shown in Figure 2B, are crystal defects and act as favorable sites or surfaces for nucleation of new phases such as pigeonite or melt (Nicholson, 1968). The predicted ease of nucleation of new phases on dislocations adjacent to the augite lamellae would suggest that our observed temperatures of first appearance of pigeonite, in samples that contain both orthopyroxene and augite, are close to the minimum temperature of the volume in which three pyroxenes are stable at this composition.

Sample 29 consists of chemically homogeneous gem-quality orthopyroxene ($Ca_{0.012}Mg_{1.636}Fe_{0.352}Si_2O_6$) containing no included augite or other phases as determined by both light optical and transmission electron microscopy. The sample is less magnesian than sample 3 and therefore would be expected, if augite were present, to form pigeonite at an even lower temperature, approximately 1220°C, compared with the 1259° temperature observed for sample 3 (Fig. 7; Table 6). However, in the absence of augite lamellae (calcium saturation zones), sample 29 did not form pigeonite until 1375°C, 155° above the expected temperature. Obviously, the temperature at which pigeonite first appears depends not only on the iron–magnesium ratio, but also on the local calcium content and on the presence of favorable nucleation sites. At temperatures as high as 1382°C, melting was not observed in this pyroxene. Orthopyroxene sample 30, which also did not contain any augite, behaved similarly in that pigeonite appeared at 1360°C rather than at 1212°C, the minimum temperature expected for three-pyroxene equilibrium at this bulk composition. The lack of favorable nucleation sites in these two precipitate-free orthopyroxenes (29, 30) could also delay the appearance of melt, although we are certain that the low calcium concentration contributes to the high melting point.

Comparison with previous work

We did not attempt to determine the minimum stability temperature of iron-free pigeonite in this investigation. Extrapolation of the data in Figure 7 to [Mg] = 100 suggests that ~1300°C is the temperature at which iron-free orthopyroxene + augite react to form pigeonite. This temperature compares well with the value of 1278±10°C (converted to IPTS '68) reported by Yang (1973) for the equilibrium assemblage orthorhombic pyroxene–augite–pigeonite. Yang originally designated this orthorhombic phase as "protoenstatite." However, his observations by optical methods were sufficient only to indicate an orthorhombic symmetry (oral communication, 1973), which is not sufficient evidence to distinguish between orthopyroxene (*Pbca*) and protopyroxene (*Pbcn*). In view of the absence of cracks and polysynthetic twinning in his quenched "protoenstatite" (Yang, 1973, p. 492) and the relatively calcic nature of this phase (2.4 weight

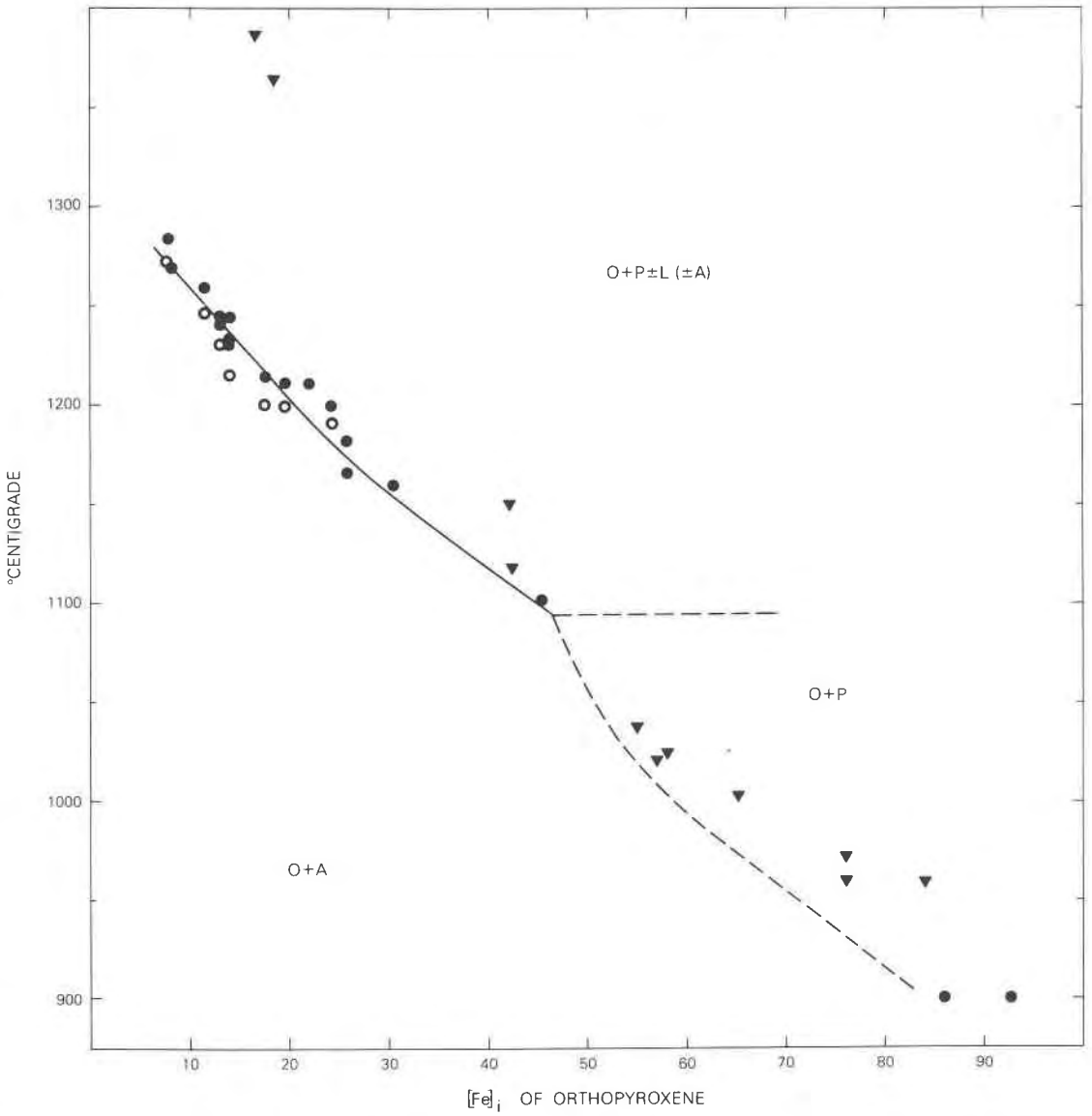

Fig. 7. Summary of experimental results using orthopyroxene at one bar. Individual data points are listed in Table 6. Closed circles indicate orthopyroxene in which augite was observed to coexist with pigeonite. Open circles indicate orthopyroxenes in which augite was detected, but pigeonite was not observed. Triangles designate orthopyroxenes in which no augite was observed with the appearance of pigeonite; the triangle points in the direction in which the 3-pyroxene equilibrium must lie. The solid line, which is thought to be close to equilibrium, is not reversed. The dashed lines are not well located by our experiments, and are thus intended to be schematic.

percent CaO; p. 493), we favor the interpretation that the orthorhombic pyroxene in question is orthopyroxene (*Pbca*).[3] Comparison of the results is then limited only by the aforementioned extrapolation to zero iron content and the fact that Yang used pure, synthetic starting materials in the system $CaO–MgO–SiO_2–Al_2O_3$, whereas our starting materials were natural pyroxene crystals that contained small amounts of TiO_2, MnO, Na_2O, *etc.*

Comparison with the work of Bowen and Schairer (1935) is difficult because of uncertainties in the nature of the phases they produced in their experiments. Enstatite from the Bishopville meteorite, [Fe] = 0.6, reacted at 1145°C to produce

[3]"Protoenstatite" is rarely, if ever, quenched without some or all of the crystallites reacting to form pigeonite ("clinoenstatite"). In our experience such crystallites always possess a very characteristic texture which includes polysynthetic twinning and large prominent cracks, the latter caused by the large volume difference between "protoenstatite" and "clinoenstatite."

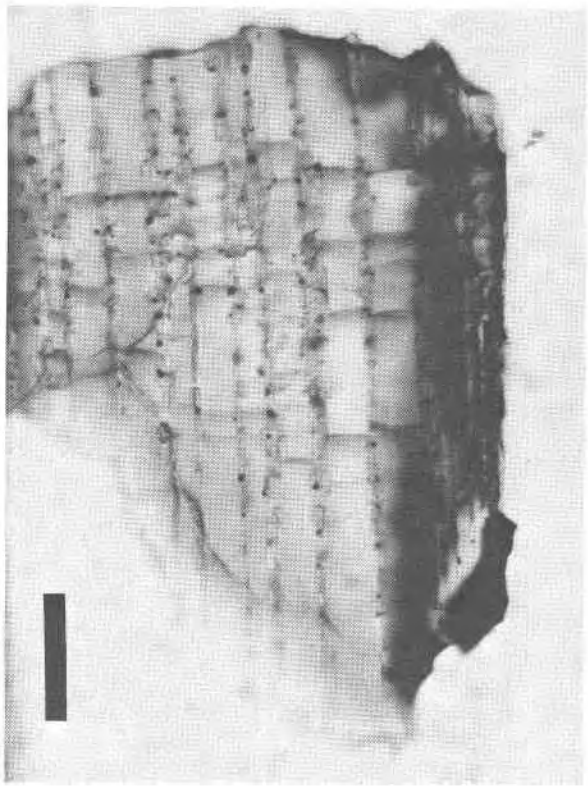

Fig. 8. Orthopyroxene (sample 3 run at 1332°C), containing bands (7–20 μm wide) of pigeonite + blebs of glass (quenched partial melt; note the "bubbles" possibly formed by contraction of liquid on cooling or by evolution of volatiles). Compositions of phases are given in Table 4 and plotted in Fig. 5. The observed pigeonite + glass are inferred to have formed by reaction of host orthopyroxene with augite along augite lamellar interfaces (see text). Bar scale is 0.1 mm.

a quenched product identified as twinned clinopyroxene. This temperature is too low for the reaction of orthopyroxene + augite to yield pigeonite. We suggest that the meteoritic orthopyroxene was never at calcium saturation (contained no augite) and that Bowen and Schairer observed twinned pigeonite that formed from protopyroxene on quenching from 1145°C. Bowen and Schairer heated the two bronzite samples, [Fe] = 13.5, 13.8, with NaF flux to assist the transformation of orthopyroxene to pigeonite. Their reported transformation temperature, 1120°C, is 117° below the temperature that we would predict from Figure 7 for the first appearance of pigeonite. We suspect that the observed reaction is the formation of monoclinic fluoramphibole, not a clinopyroxene. We are disturbed by the observation (p. 167) that, in the absence of flux, the "two bronzites can be heated for hours at temperatures more than 300° above their true inversion temperature, even at temperatures where they are partly melted, without visible transformation." In our experience, pigeonite is commonly not readily detected without an X-ray precession photograph. The transformation temperatures reported by Bowen and Schairer for their two iron-rich orthopyroxenes, [Fe] = 47.3 and 80.4, are 1090° and 955°C; these values are slightly higher than those produced in our own work. Our method detects small amounts of pigeonite first formed at regions of augite saturation. Bowen and Schairer presumably could not detect pigeonite until the transformation had proceeded to a greater extent. Thus, their observed transformation temperatures are slightly higher than our predicted values.

Ishii (1975) relates the minimum temperature of pigeonite stability to the Fe/(Mg+Fe) ratio (X_{Fe}) of pigeonite by the single expression $T°C = 1270 - 480X_{Fe}$. This expression is based on the experimental work of Yang (1973) and Brown (1968), and on two temperature measurements of eruptive flows from Japanese volcanoes. Pigeonite compositions were obtained from electron microprobe analyses of ejecta materials. Ishii's expression gives temperatures ~25°C lower than the temperatures of our runs, in basic agreement with our results. We do not believe, however, that temperature measurements of extruded lava clearly give a close approximation to the temperature of phenocryst crystallization. Furthermore, the electron probe composition must be carefully chosen to reflect the composition of pigeonite which *coexists* with augite and orthopyroxene. The pigeonite compositions given by Ishii (1975, Table 1, samples 3109, 3111, 3114) for the Mihara-yama occurrence are clearly too calcic to have been in equilibrium with the adjacent orthopyroxene.

Effects of nonhydrostatic stress and hydrostatic pressure

Recent experimental studies have cast uncertainty upon the true stability relationships of orthopyroxene and pigeonite at low temperature. Riecker and Rooney (1967) and Coe (1970) show that under shearing stress, orthopyroxene transforms at low temperature to "clinoenstatite" similar to that observed by Sclar *et al.* (1964) and Boyd and England (1965). Raleigh *et al.* (1971) consider the "clinoenstatite" to be metastable with respect to orthopyroxene under hydrothermal conditions. Grover (1972) "reversed" the ortho–clinopyroxene reaction in $MgCl_2 \cdot H_2O$ flux and found the opposite result, that at temperatures *below* 556°C "clinoenstatite" is stable relative to orthopyroxene. We

assume that this low-temperature "clinoenstatite" is a very magnesium-rich, calcium-poor pigeonite with $P2/c$ symmetry, but a thorough characterization of this experimentally-produced phase has not been made. Coe and Kirby (1975) state that shearing expands the "clinoenstatite" stability field, and in the "clinoenstatite" field increases the rate at which orthopyroxene transforms to the stable "clinoenstatite." The above results are indeed puzzling because orthopyroxene is the *naturally*-occurring low-temperature, calcium-poor pyroxene, formed in a variety of environments, many of which were undoubtedly under resolved shear stress on (100) as they cooled through the purported "clinoenstatite" field. For example, enstatite from Bamble, Norway, of composition $Ca_{0.004}Mg_{1.930}Fe_{0.066}Si_2O_6$ shows partial alteration to talc but no low-temperature "clinoenstatite" phase appears in the single-crystal X-ray photographs.

Several efforts have been made to determine the pigeonite stability field at hydrostatic pressures of 1 to 3 kbar H_2O. Lindsley *et al.* (1973) established that pigeonite with Fe/(Mg+Fe) approximately equal to 0.80 decomposed to orthopyroxene + augite at 700°C and 3 kbar. Simmons *et al.* (1974), using a bulk composition with Fe/(Mg+Fe) = 0.75, grew pigeonite (+ olivine + quartz) from orthopyroxene + augite at 800°C (2 kbar), and decomposed pigeonite into orthopyroxene + augite at 800°C (2 kbar) and 750°C (3 kbar), thereby reversing the reaction within a narrow but unknown range of Fe/(Mg+Fe). Podpora and Lindsley (1979) used a mixture of synthetic powdered orthopyroxene and augite, with bulk Fe/(Mg+Fe) = 0.75, to crystallize pigeonite at 2 kbar and both 825° and 850°C. With bulk Fe/(Mg+Fe) = 0.60, they were able to form pigeonite at 900°C. Thus it appears possible to grow iron-rich pigeonites at temperatures that are lower than suggested by the runs in Figure 7.

At high pressure, under conditions believed to be close to hydrostatic, the minimum temperature for the pigeonite field is known only at 15 kbar and for Fe/(Mg+Fe) > 0.6 (Fig. 9). For bulk compositions with Fe/(Mg+Fe) = 0.84, the temperature is in the range 875°–900°C (Smith, 1972); for Fe/(Mg+Fe) = 0.60 and 0.75 the temperatures are, respectively, 1005°±10°C and 900°±20°C (Grover *et al.*, 1972). The same starting materials were used for the Fe/(Fe+Mg) = 0.75 experiments at 2 kbar (Simmons *et al.*, 1974) and 15 kbar (Grover *et al.*, 1972), and the same criteria were used to interpret the results (D. H. Lindsley, personal communication, 1978). Thus, these results should be optimum for determining the $(\partial T/\partial P)_{[Fe]}$ of reaction, and the result is 8°C kbar^{-1}.

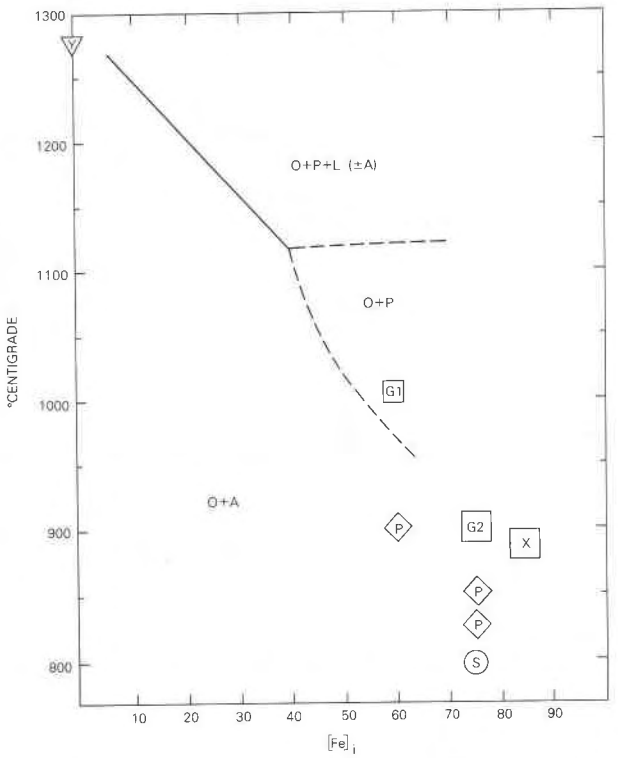

Fig. 9. Summary of our results (Fig. 7) compared with previous experimental results. At one atmosphere: "Y" designates Yang (1973), orthorhombic pyroxene to pigeonite (discussed in text). At 1–3 kbar, "S" designates Simmons *et al.* (1974), and "P" indicates Podpora and Lindsley (1979). At 15 kbar "G1" and "G2" designate Grover *et al.* (1972) and "X" designates Smith (1972).

Possible difficulties

Evaluation of the Clapeyron equation, $(dT/dP) = (\Delta V/\Delta S)$ may help explain the relatively high temperature that we found for formation of iron-rich pigeonite, relative to other investigators. The molar volume of reaction calculated from unit-cell data of the three pyroxene phases measured in the same laboratory (Turnock *et al.*, 1973) is only 0.05 cm^3 mole^{-1} for the reaction orthopyroxene + augite = pigeonite at Fe/(Fe+Mg) ≃0.75 (at standard P and T). This molar volume of reaction, combined with the observed (dT/dP) of 8°C kbar^{-1}, yields an entropy of reaction (ΔS_R) of only 0.15 cal deg^{-1} mole^{-1}. That the ΔS_R value is small is undoubtedly due to the similarity of the orthopyroxene, pigeonite, and augite structures. The ΔS_R would be dominated by contributions from changing the cell size from 18A in orthopyroxene to 9A in clinopyroxene and

from rearranging atoms in the octahedral (M) sites. Because blocks of atoms are rearranged in changing from *Pbca* to *C2/c* (or $P2_1/c$) symmetry, and because only a small proportion of the cations redistribute themselves among similar sites, we expect the entropy change associated with pigeonite growth from orthopyroxene + augite to be small.[4] In this situation the entropy associated with defects such as the dislocations we showed in Figure 2b may be a significant component of the entropy of reaction. If so, the nature and location of defects could influence the conditions at which pigeonite forms in laboratory experiments, and in nature. Likewise the existence of a structurally disordered pyroxene phase or pyriboles, as proposed by Veblen *et al.* (1977), could influence the results.

We conclude that the temperature at which iron-rich orthopyroxene [Fe/(Fe+Mg) > 0.45] first reacts with included augite is not known with certainty. We are confident, however, that existing experimentation at low pressure ($P < 2$ kbar) provides limits for the reaction in the laboratory and in nature. The upper limit for the minimum temperature of pigeonite formation must lie at lower temperatures than our runs in which pigeonite, but not augite, was detected in orthopyroxene host. The upper limit cannot lie at greater temperatures than those of our runs in which *both* pigeonite and augite were detected in the orthopyroxene. The experiment of Simmons *et al.* (1974) provides a lower temperature limit of 800°C at Fe/(Mg+Fe) ≅ 0.75. It is possible that there is no unique temperature–composition relationship for the reaction. There might be minor but unrecognized variations with changes in minor-element chemistry, and there is a good possibility that the temperature at which the reaction is initiated will depend upon the fine structure of the reactants.

Uncertainty in the temperature at which iron-rich orthopyroxene + augite react to form pigeonite prompts a note of caution. The 3-pyroxene assemblages reported by Ross and Huebner (1975b) at Fe/(Mg+Fe) > 0.55 were based on the lowest temperature at which pigeonite was observed. Augite did not always coexist with orthopyroxenes in these runs at Fe/(Mg+Fe) > 0.55; their reported subsolidus geothermometer should be regarded as yielding maximum possible temperatures.

[4]A similar relationship exists between the two-layer clay mineral dickite and its one-layer polymorph kaolinite, which differ in $S^\circ_{289.15}$ by only 1.4±0.6 cal deg^{-1} mole^{-1} (King and Weller, 1961). At least some of this entropy change may be due to rearrangement of the hydrogen bonds between the layers.

Epilogue

We report these results as an attempt to outline the phase relations of calcium-poor pyroxenes. Rather than being the final word on the subject, we believe the data for Mg-rich compositions to be more secure than the data for more Fe-rich pyroxenes. It is clear that we advocate phase characterization by single-crystal X-ray diffraction methods, and encourage greater use of electron microscopy—for ourselves and others.

Our experimental results show that it is possible to retain the bulk composition of single crystals, even when melt is present, during an experiment of at least several days' duration. We have also demonstrated the utility of the X-ray precession camera to detect small amounts of pigeonite in the run products—amounts that cannot be proven by X-ray powder diffraction. We present what we believe is close to an equilibrium between magnesian orthopyroxene, pigeonite and melt; however, we recognize that the orthopyroxene–pigeonite boundary for *our* iron-rich pyroxenes lies at lower temperatures than the runs in which we detected pigeonite. We hope that future investigators will better determine these reactions and evaluate the many possible variables.

Acknowledgments

We thank our colleagues at the U.S. Geological Survey for their help in this study: Lovell B. Wiggins and Nelson Hickling assisted in analyzing some of the pyroxenes; Mary Woodruff processed much microprobe data through the computer and desk calculator, and assisted in assembly of the bibliography and typing of the manuscript; Gordon L. Nord, Jr., provided the transmission electron photomicrograph of the dislocations, Figure 2B, and gave us much help with his knowledge of subsolidus reactions in silicates. David R. Wones, G. L. Nord, D. H. Lindsley, and D. G. Smith provided technical reviews of the manuscript. We are particularly grateful for the thorough and penetrating review by Lindsley. This research was supported in large part by NASA contract T-2356A.

References

Atkins, F. B. (1969) Pyroxenes of the Bushveld intrusion, South Africa. *J. Petrol., 10,* 222–249.

Barker, F. (1964) Sapphirine-bearing rock, Val Codera, Italy. *Am. Mineral., 49,* 146–152.

Binns, R. A. (1962) Metamorphic pyroxenes from the Broken Hill district, New South Wales. *Mineral. Mag., 33,* 320–338.

Bowen, N. L. and J. F. Schairer (1935) The system MgO–FeO–SiO_2. *Am. J. Sci., 29,* 151–217.

Boyd, F. R. and J. L. England (1965) The rhombic enstatite–clinoenstatite inversion. *Carnegie Inst. Wash. Year Book, 64,* 117–123.

——— and D. Smith (1971) Compositional zoning in pyroxenes

from lunar rock 12021, Oceanus Procellarum. *J. Petrol., 12,* 439–464.

Brown, G. M. (1957) Pyroxenes from the early and middle stages of fractionation of the Skaergaard intrusion, East Greenland. *Mineral. Mag., 31,* 511–543.

——— (1968) Experimental studies on inversion relations in natural pigeonitic pyroxenes. *Carnegie Inst. Wash. Year Book, 66,* 347–353.

——— and E. A. Vincent (1963) Pyroxenes from the late stages of fractionation of the Skaergaard intrusion, East Greenland. *J. Petrol., 4,* 175–197.

Butler, P. (1969) Mineral compositions and equilibria in the metamorphosed iron formation of the Gagnon region, Quebec, Canada. *J. Petrol., 10,* 56–101.

Cameron, E. N. (1963) Structure and rock sequences of the critical zone of the Eastern Bushveld Complex. *Mineral. Soc. Amer. Spec. Pap., 1,* 93–107.

Coe, R. S. (1970) The thermodynamic effect of shear stress on the ortho–clino inversion in enstatite and other coherent phase transitions characterized by a finite simple shear. *Contrib. Mineral. Petrol., 2,* 247–264.

——— and S. H. Kirby (1975) The orthoenstatite to clinoenstatite transformation by shearing and reversion by annealing: mechanism and potential applications. *Contrib. Mineral. Petrol., 52,* 29–55.

Dallwitz, W. B., D. H. Green and J. E. Thompson (1966) Clinoenstatite in a volcanic rock from the Cape Vogel area, Papua. *J. Petrol., 7,* 375–403.

Davidson, L. R. (1968) Variation in ferrous iron–magnesium distribution coefficients of metamorphic pyroxenes from Quairading, western Australia. *Contrib. Mineral. Petrol., 19,* 239–259.

Desborough, G. A., and H. J. Rose, Jr. (1968) X-ray and chemical analysis of orthopyroxenes from the lower part of the Bushveld Complex, South Africa. In *Geological Survey Research 1968: U.S. Geol. Surv. Prof. Paper, 600-B,* B1–B5.

Dodd, R. T., J. E. Grover and G. E. Brown (1975) Pyroxenes in the Shaw (L-7) chondrite. *Geochim. Cosmochim. Acta, 39,* 1585–1594.

Gooley, R., R. Brett and J. L. Warner (1974) A lunar rock of deep crustal origin: sample 76534. *Geochim. Cosmochim. Acta, 38,* 1329–1339.

Grover, J. (1972) The stability of low-clinoenstatite in the system $Mg_2Si_2O_6$–$CaMgSi_2O_6$ (abstr.). *Trans. Am. Geophys. Union, 53,* 539.

———, D. H. Lindsley and A. C. Turnock (1972) Ca–Mg–Fe pyroxenes: subsolidus phase relations in iron-rich portions of the pyroxene quadrilateral (abstr.). *Geol. Soc. Am. Abstracts with Programs, 4,* 521–522.

Heald, E. F. (1967) Thermodynamics of iron–platinum alloys. *Trans. Met. Soc. AIME, 239,* 1337–1340.

Huebner, J. S. (1973) Experimental control of wüstite activity and mole fraction (abstr.). *Geol. Soc. Am. Abstracts with Programs, 5,* 676–677.

——— (1975) Oxygen fugacity values of furnace gas mixtures. *Am. Mineral., 60,* 815–823.

———, B. R. Lipin and L. B. Wiggins (1976) Partitioning of chromium between silicate crystals and melt. *Proc. Lunar Sci. Conf. 7th,* 1195–1220.

———, M. Ross and N. Hickling (1975) Significance of exsolved pyroxenes from lunar breccia 77215. *Proc. Lunar Sci. Conf. 6th,* 529–546.

———, ———, ——— and A. C. Turnock (1972) Partial melting of pyroxenes and the origin of mare basalts. *Lunar Sci. IV,* 397–399. Lunar Science Institute, Houston, Texas.

Immega, I. P. and C. Klein, Jr. (1976) Mineralogy and petrology of some metamorphic Precambrian iron-formations in southwestern Montana. *Am. Mineral. 61,* 1117–1144.

Ishii, T. (1975) The relations between temperature and composition of pigeonite in some lavas and their application to geothermometry. *Mineral. J., 8,* 48–57.

Ito, J. (1976) Experimental studies of $Li^+ + Sc^+$ coupled substitution in the Mg-silicates: olivine, clinopyroxene, orthopyroxene, protoenstatite and a new high temperature phase with $c = 27$A (abstr.). *Geol. Soc. Am. Abstracts with Programs, 8,* 937–938.

Jaffe, H. W., P. Robinson, R. J. Tracy and M. Ross (1975) Orientation of pigeonite exsolution lamellae in metamorphic augite: correlation with composition and calculated optimal phase boundaries. *Am. Mineral., 60,* 9–28.

King, E. G. and W. W. Weller (1961) Low-temperature heat capacities and entropies at 298.15°K of diaspore, kaolinite, dickite and halloysite. *U.S. Bur. Mines Rept. Inv. 5810.*

Klein, C. (1966) Mineralogy and petrology of the metamorphosed Wabush Iron Formation, southwestern Labrador. *J. Petrol., 7,* 246–305.

Kuno, H. (1954) Study of orthopyroxenes from volcanic rocks. *Am. Mineral., 39,* 30–46.

Larsen, E. S., Jr., and W. M. Draisin (1950) Composition of the minerals in the rocks of the southern California batholith. *Intern. Geol. Congress, 18th Session,* Pt. 11, 66–79.

Lindsley, D. H., J. E. Grover and C. E. Calabro (1973) Subsolidus phase relations of Ca–Mg–Fe pyroxenes with Fe/Fe+Mg near 0.75 at pressures from 1–5 kbar and temperatures from 600–800°C (abstr.). *Geol. Soc. Am. Abstracts with Programs, 5,* 713–714.

Mason, B. and E. Jarosewich (1971) The composition of the Johnstown meteorite. *Meteoritics, 6,* 241–245.

Nakamura, Y. and I. Kushiro (1970a) Equilibrium relations of hypersthene, pigeonite, and augite in crystallizing magma: microprobe study of a pigeonite andesite from Weiselberg, Germany. *Am. Mineral., 55,* 1999–2015.

——— and ——— (1970b) Compositional relations of coexisting orthopyroxene, pigeonite, and augite in a tholeiitic andesite from Hakone Volcano. *Contrib. Mineral. Petrol., 26,* 265–275.

Nicholson, R. B. (1968) Nucleation at imperfections. In *Phase Transformations,* p. 269–312. American Society of Metals Seminar Publication, New York.

Papike, J. J., F. N. Hodges, A. E. Bence, M. Cameron and J. M. Rhodes (1976) Mare basalts: crystal chemistry, mineralogy, and petrology. *Rev. Geophys. Space Phys., 14,* 475–540.

Podpora, C. and D. H. Lindsley (1979) Fe-rich pigeonites: minimum temperatures of stability in the Ca–Mg–Fe quadrilateral (abstr.). *Trans. Am. Geophys. Union, 60,* 420–421.

Raleigh, C. B., S. H. Kirby, N. L. Carter and H. G. Ave Lallemant (1971) Slip and the clinoenstite transformation as competing rate processes in enstatite. *J. Geophys. Res., 76,* 4011–4022.

Ramberg, H. and G. W. Devore (1951) The distribution of Fe^{2+} and Mg^{2+} in coexisting olivines and pyroxenes. *J. Geol., 59,* 193–210.

Riecker, R. E. and T. P. Rooney (1967) Deformation and polymorphism of enstatite under shear stress. *Geol. Soc. Am. Bull., 78,* 1045–1054.

Rietmeijer, F. J. M. (1979) *Pyroxenes from Iron-rich Igneous*

Rocks in Rogaland, S.W. Norway. Ph.D. Dissertation, Utrecht University, The Netherlands.

Ross, M. (1968) X-ray diffraction effects by non-ideal crystals of biotite, muscovite, montmorillonite, mixed-layer clays, graphite, and periclase. *Z. Kristallogr., 126,* 80–97.

——— and J. S. Huebner (1975a) Estimation of the minimum temperature for existence of orthopyroxene, pigeonite, and augite and its application to prediction of temperature of crystallization of lunar pyroxenes. *Lunar Sci. VI,* 689–691. Lunar Science Institute, Houston, Texas.

——— and ——— (1975b) A pyroxene geothermometer based on composition–temperature relationships of naturally occurring orthopyroxene, pigeonite, and augite (abstr.). Extended Abstracts, *International Conference on Geothermometry and Barometry.* Pennsylvania State University, University Park, Pennsylvania.

———, ——— and E. Dowty (1973) Delineation of the one-atmosphere augite–pigeonite miscibility gap for pyroxenes from lunar basalt 12021. *Am. Mineral., 58,* 619–635.

———, ——— and N. L. Hickling (1972) Delineation of the orthopyroxene–pigeonite transition and its bearing on pyroxene phase relations in lunar rocks. *Lunar Sci. IV,* 637–639. Lunar Science Institute, Houston, Texas.

Sclar, C. B., L. C. Carrison and C. M. Schwartz (1964) High-pressure stability field of clinoenstatite and the orthoenstatite–clinoenstatite transition (abstr.). *Trans. Am. Geophys. Union, 45,* 121.

Simmons, E. C., D. H. Lindsley and J. J. Papike (1974) Phase relations and crystallization sequence in a contact-metamorphosed rock from the Gunflint Iron Formation, Minnesota. *J. Petrol., 15,* 539–65.

Smith, D. (1972) Stability of iron-rich pyroxene in the system $CaSiO_3$–$FeSiO_3$–$MgSiO_3$. *Am. Mineral., 57,* 1413–1428.

——— (1974) Pyroxene–olivine–quartz assemblages in rocks associated with the Nain Anorthosite Massif, Labrador. *J. Petrol., 15,* 58–78.

Smith, J. V. (1959) The crystal structure of protoenstatite, $MgSiO_3$. *Acta Crystallogr., 12,* 515–519.

Smyth, J. R. (1969) Orthopyroxene–high–low clinopyroxene inversions. *Earth Planet. Sci. Lett., 6,* 406–407.

——— and J. Ito (1977) The synthesis and crystal structure of a magnesium–lithium–scandium protopyroxene. *Am. Mineral., 62,* 1252–1257.

Stewart, D. B., M. Ross, B. A. Morgan, D. E. Appleman, J. S. Huebner and R. F. Commeau (1972). Mineralogy and petrology of lunar anorthosite 15415. *Lunar Sci. III,* 726–728. Lunar Science Institute, Houston, Texas.

Subramaniam, A. P. (1962) Pyroxenes and garnets from charnockites and associated granulites. In A. E. J. Engel, H. L. James and B. F. Leonard, Eds., *Petrologic Studies: A Volume to Honor A. F. Buddington,* p. 21–36. Geological Society of America, New York.

Turnock, A. C., D. H. Lindsley and J. E. Grover (1973) Synthesis and unit-cell parameters of Ca–Mg–Fe pyroxenes. *Am. Mineral., 58,* 50–59.

Veblen, D. R., P. R. Buseck and C. W. Burnham (1977) Asbestiform chain silicates: new minerals and structural groups. *Science, 198,* 359–366.

Virgo, D. and M. Ross (1973) Pyroxenes from Mull andesites. *Carnegie Inst. Wash. Year Book, 72,* 535–540.

Wager, L. R. and W. A. Deer (1939) Geological investigation in East Greenland. Part III. The petrology of the Skaergaard Intrusion, Kangerdlugssuag, East Greenland. *Medd. om Grønland, 105,* 1–352.

Yang, H. Y. (1973) Crystallization of iron-free pigeonite in the system anorthite–diopside–enstatite–silica at atmospheric pressure. *Am. J. Sci., 273,* 488–497.

Manuscript received, December 19, 1977;
accepted for publication, July 9, 1979.